Biogeochemistry (2019) 146:145–170
https://doi.org/10.1007/s10533-019-00613-1

Si cycling in transition zones: a study of Si isotopes and biogenic silica accumulation in the Chesapeake Bay through the Holocene

Carla K. M. Nantke · Patrick J. Frings · Johanna Stadmark · Markus Czymzik · Daniel J. Conley

Received: 11 March 2019 / Accepted: 11 October 2019 / Published online: 25 November 2019

Abstract Si fluxes from the continents to the ocean are a key element of the global Si cycle. Due to the ability of coastal ecosystems to process and retain Si, the 'coastal filter' has the potential to alter Si fluxes at a global scale. Coastal zones are diverse systems, sensitive to local environmental changes, where Si cycling is currently poorly understood. Here, we present the first palaeoenvironmental study of estuarine biogenic silica (BSi) fluxes and silicon isotope ratios in diatoms ($\delta^{30}Si_{diatom}$) using hand-picked diatom frustules in two sediment cores (CB_{dist} and CB_{prox}) from the Chesapeake Bay covering the last 12000 and 8000 years, respectively. Constrained by the well-understood Holocene evolution of the Chesapeake Bay, we interpret variations in Si cycling in the context of local climate, vegetation and land use changes. $\delta^{30}Si_{diatom}$ varies between + 0.8 and + 1.7‰ in both sediment cores. A Si mass balance for the Chesapeake Bay suggests much higher rates of Si retention (~ 90%) within the system than seen in other coastal systems. BSi fluxes for both sediment cores co-vary with periods of sea level rise (between 9500 and 7500 a BP) and enhanced erosion due to deforestation (between 250 and 50 a BP). However, differences in $\delta^{30}Si_{diatom}$ and BSi flux between the sites emphasize the importance of the seawater/freshwater mixing ratios and locally variable Si inputs from the catchment. Further, we interpret variations in $\delta^{30}Si_{diatom}$ and the increase in BSi fluxes observed since European settlement (~ 250 a BP) to reflect a growing human influence on the Si cycle in the Chesapeake Bay. Thereby, land use change, especially deforestation, in the catchment is likely the major mechanism.

Keywords Diatoms · Estuarine sediments · Human impact · Si isotopes

Responsible Editor: Maren Voss.

C. K. M. Nantke (✉) · J. Stadmark · D. J. Conley
Lund University, Quaternary Geology, Sölvegatan 12, 22362 Lund, Sweden
e-mail: carla.nantke@geol.lu.se

P. J. Frings
GFZ German Research Centre for Geosciences, Section 3.3 Earth Surface Geochemistry, Telegrafenberg, 14473 Potsdam, Germany

P. J. Frings
Department of Geosciences, Swedish Museum of Natural History, Frescativägen 40, 10405 Stockholm, Sweden

M. Czymzik
Leibniz Institute for Baltic Sea Research Warnemünde (IOW), Seestraße 15, 18119 Rostock, Germany

Introduction

Silicon (Si) is the second most abundant element in the Earth's crust (28%) and is coupled to the global carbon cycle (Berner 1992). On geological timescales, the

weathering of silicate minerals consumes atmospheric CO_2 by generating bicarbonate (Walker et al. 1981) which subsequently precipitates as carbonate minerals in the ocean. Diatoms—siliceous phytoplankton—play a major role in the uptake and transport of carbon in the water column and its sequestration in marine sediments (the 'biological pump') (Honjo et al. 2008).

In the last decades, multiple studies have examined the impact of climate and ecosystem changes on the terrestrial and marine Si cycles (Conley et al. 2008; Struyf et al. 2009). Frings et al. (2016) summarized potential changes to the ocean Si budget since the Last Glacial Maximum (LGM, ca. 21 ka BP). These include variations in the river dissolved Si (DSi) and particulate Si (PSi) fluxes due to changes in the continental Si cycle, the dust flux and weathering rates. An imbalance between the best estimates of the sources and sinks in the ocean Si budget serves to highlight our poor understanding of transition zones between the terrestrial and oceanic realms (Tréguer and De La Rocha 2013; Frings et al. 2016). In these zones, the nature and magnitude of Si delivered to the ocean can be altered (Dürr et al. 2011), but it is unclear where and by how much. We can reduce this knowledge gap by identifying and quantifying the processes controlling the removal, retention or recycling of Si in coastal zones.

Si isotopes

Silicon isotope ratios (expressed as $\delta^{30}Si$) are a powerful tool for the analysis of shifts in Si budgets in response to climate and vegetation changes (Leng et al. 2009; Sun et al. 2011; Frings et al. 2014b, 2016). The distribution of the three stable isotopes of Si (^{28}Si, ^{29}Si and ^{30}Si) changes subtly due to isotope fractionation induced by a variety of processes, including weathering, clay formation or Si utilization by terrestrial plants and aquatic organisms (notably diatoms, but also radiolarians and sponges). Diatoms are the dominant silicifying organism in many aquatic systems, and discriminate against the heavier isotopes of silicon during the production of their frustules, with a fractionation of approximately – 1.1‰ (De la Rocha et al. 1997). This preferential uptake of the lighter ^{28}Si leaves their environment correspondingly enriched in the heavier ^{30}Si. Mass balance models require that the silicon isotope ratios of both diatom silica ($\delta^{30}Si_{diatom}$) and the residual dissolved Si ($\delta^{30}Si_{diss}$) vary systematically as a function of the degree of conversion of dissolved Si to diatom silica (Varela et al. 2004), forming the basis of $\delta^{30}Si_{diatom}$ as a palaeoproductivity proxy.

This interpretation of $\delta^{30}Si_{diatom}$ assumes a constant (or at least known) $\delta^{30}Si_{diss}$ of the source Si. This assumption has been challenged even in the open ocean over millennial timescales (Frings et al. 2016). In more dynamic coastal zones, it is almost certainly invalid. Here, $\delta^{30}Si_{diss}$ can vary depending on a suite of upstream processes determining Si export from terrestrial sources, and can subsequently be modified by DSi utilization by diatoms. To deconvolve the two competing influences on $\delta^{30}Si_{diatom}$, an independent constraint on diatom production would be useful. This could be achieved though the determination of biogenic Si (BSi) fluxes as a proxy for diatom production. These fluxes are influenced by various parameters, controlling diatom production like nutrient inputs, salinity and pH in the euphotic zone and those that control diatom frustule deposition and recycling rates like the composition of the food web, water pH, and oxygen conditions in the deeper water layers (Sun et al. 2014).

The flux of DSi transported to the ocean is ultimately set by the weathering rate of silicate minerals, but can be modified by changes in the amount of Si stored in the terrestrial soil–plant system, and the various 'fluvial filters' (including soil systems, wetlands, estuaries) it must traverse before reaching the ocean (Meybeck and Vörösmarty 2005; Struyf and Conley 2012). These filters have been shown to alter Si isotope ratios during the transport of Si from the initial weathering process until its delivery to the ocean. In estuaries Si utilization and deposition by diatoms most likely reduces the river-ocean DSi flux. Reverse weathering—the in situ formation of new aluminosilicate minerals—in coastal zone sediments can further reduce the land–ocean Si flux (Krause et al. 2017; Rahman et al. 2017). Estimates of global DSi fluxes from terrestrial ecosystems to the oceans are on the order of 7×10^{12} mol (Tmol a^{-1}) (e.g. 6.3 Tmol Si a^{-1} (Beusen et al. 2009) and 7.3 Tmol Si a^{-1} (439 Mt a^{-1}) (Tréguer and De La Rocha 2013)). Including particulate Si (PSi) yields a total annual flux of 153 Tmol a^{-1} (9206 Mt a^{-1}) (with 6 Tmol DSi a^{-1} (371 Mt a^{-1}) plus 147 Tmol PSi a^{-1} (8835 Mt a^{-1}) (Dürr et al. 2011), though the common assumption is that this PSi is relatively unreactive.

The terrestrial Si cycle

Because plant uptake is one of the largest fluxes in the global Si cycle (Conley 2002), terrestrial Si cycling is strongly influenced by the local vegetation at a given site. It might be expected to vary following e.g. ecosystem succession or perturbations. Plants use Si to produce phytoliths—microscopic amorphous silica bodies that convey structural, physiological and ecological benefits to the plant—but the usage changes with vegetation type. For example, grasses and crop species have an particularly high demand for Si (Carey and Fulweiler 2012). When the plant dies, the amorphous Si (ASi)—a biogenic form of Si, susceptible to dissolution—is returned to the soil where it is either dissolved, eroded or stored (Frings et al. 2014a). The dissolved ASi can be further recycled by local vegetation, or lost to the fluvial system. ASi will accumulate in soils when its supply by litterfall exceeds its dissolution and export rates (Struyf et al. 2010). In contrast, a decreasing Si supply (which might be induced by vegetation change), can lead to diminishing soil ASi pools. In general, ecosystem disturbances tend to decrease the recycling of ASi, and consequently increase Si export rates and decrease the size of the soil ASi reservoir (Struyf et al. 2010; Clymans et al. 2011).

Additional impacts on the terrestrial Si cycle are caused by human activities (Struyf and Conley 2012; Vandevenne et al. 2015). For example, it has been shown that deforestation leads to an abrupt export of Si from the ASi pool to the soil- and groundwater (Conley et al. 2008; Vandevenne et al. 2015). $\delta^{30}Si$ measurements of soil waters have revealed the impact of changes in vegetation, land use and hydrology on the terrestrial Si cycle (Vandevenne et al. 2015). Diminished ASi storage in soil systems was attributed to increasing Si harvest and erosion of surface soils. A shift of $\delta^{30}Si$ towards heavier values can be linked to the depletion in light isotopes in cultivated landscapes. Vandevenne et al. (2015) further showed that BSi dissolution and the release of light ^{28}Si back to the soil, is of minor importance in areas dominated by cropland since the harvest of plants lead to lower recycling rates at the vegetation-soil interface. Agriculture has been found to increase the $\delta^{30}Si_{diss}$ in soil water, through the harvest of crops containing low $\delta^{30}Si$. This increase in $\delta^{30}Si_{diss}$ is also visible at the river-basin scale (Delvaux et al. 2013). Moreover, anthropogenic processes like damming, agriculture and fertilization (mainly inputs of N and P) can decrease DSi fluxes. A body of literature shows that riverine silicon isotopes faithfully record these changes. For example, damming of the Tana river triggered increased river $\delta^{30}Si_{diss}$ values (Hughes et al. 2012) (Table 1).These studies provide a conceptual and empirical framework with which to relate changes in river $\delta^{30}Si_{diss}$ to catchment Si cycling.

Si cycling in coastal zones

Due to their position between the terrestrial and oceanic compartments of the global Si cycle, coastal zone sediments are well suited to record an integrated history of catchment Si cycling, providing information on the effects of both natural environmental changes and human activity. Coastal marine areas are among the most productive ecosystems worldwide and often have a long history of human disturbances (Jickells 1998). Nutrient replete conditions favor high productivity and typically, the dominance of diatoms. Relatively short water residence times (from weeks to months) make them sensitive to environmental changes on geologically short timescales (Jickells 1998) that might be difficult to resolve in more buffered ocean waters. Major Si inputs to coastal areas are provided through terrestrial ecosystems transported via tributaries, groundwater flow and direct overland flow (Laruelle et al. 2009; Tréguer and De La Rocha 2013). The suite of climate and land use parameters that together form terrestrial Si cycling therefore determine $\delta^{30}Si_{diss}$ values in adjacent aquatic ecosystems like rivers, lakes and estuaries (Hughes et al. 2012).

Si cycling in estuaries

Observations of decreasing DSi concentrations in freshwater ecosystems in response to eutrophication (Conley et al. 1993) stimulated research on Si cycling in coastal zones (Chou and Wollast 2006). However, Si budgets in coastal areas are still relatively rare. Mangalaa et al. (2017) identified four major factors that influence the Si cycle in coastal zones: (i) lithogenic supply through changing weathering rates, (ii) diatom uptake related to population size and composition, (iii) mixing ratios of sea water and freshwater and (iv) land use changes (related to

Table 1 Summary of the hypothesized processes influencing $\delta^{30}Si_{diatom}$ in coastal ecosystems

	Process	$\delta^{30}Si_{diatom}$
Climate shift	**Enhanced precipitation**	Enhanced discharge and enhanced DSi transport to the coastal zone via rivers and ground water flows. Enhanced runoff and erosion of the Si soil pool.	Decrease in $\delta^{30}Si_{diatom}$
	Natural vegetation changes	Changes in uptake and export rates of Si in the terrestrial watershed larger export of soil stored ASi.	Decrease in $\delta^{30}Si_{diatom}$
		High demands of Si by plants can reduce the Si released to tributaries, ground waters and coastal zones.	Increase in $\delta^{30}Si_{diatom}$
	Water mixing conditions	Precipitation and freshwater delivery influences the mixing conditions in and the distribution of Si (DSi and PSi) in the water column. Marine waters have a relatively high $\delta^{30}Si_{water}$.	Depending on the location: $\delta^{30}Si_{diatom}$ increase or decrease
Human impact	**Deforestation**	Increase in Si export from the relatively light ASi pool in soils.	Decrease in $\delta^{30}Si_{diatom}$
	Land use changes	Crops have a high Si demand and leave the soil depleted in light Si isotopes. Harvest of crops reduces the release of relatively light Si stored in phytoliths back to the soil system.	Increase in $\delta^{30}Si_{diatom}$
	Damming	Slows down the discharge rate and the flow speed of the tributaries which leads to more diatom production in the river water and less DSi reaching the coastal zone.	Increase in $\delta^{30}Si_{diatom}$
	Nutrient inputs	Changes the N:P:Si ratio in an ecosystem and leads to diatom blooms or shifts in phytoplacton communities (eg. shifts from a Si saturated to a Si limited system).	Depending on the nutrient and foodweb: $\delta^{30}Si_{diatom}$ increase or decrease

changes in vegetation, soil system and hydrology). Further, reverse weathering was recently suggested to enhance the preservation efficiency of Si in coastal zones (Aller 2014; Frings et al. 2016). DSi concentrations along the salinity gradient have been investigated to better understand recent Si dynamics in coastal areas (Dürr et al. 2011; Barão et al. 2015; Mangalaa et al. 2017). A 14-year monitoring period in the Rhode River sub-watersheds of the Chesapeake Bay (hereafter 'CB') revealed inter-annual variations in Si fluxes linked to precipitation changes and water discharge (Correll et al. 2000). Dry winters were found to cause low DSi discharge and subsequent Si limitation in the Rhode River estuary (Correll et al.

2000). Seasonality in DSi supply and uptake (through diatoms in the dry season) along the pH and salinity gradient in Indian estuaries highlight the importance of freshwater/seawater mixing ratios on the Si cycle in estuaries (Mangalaa et al. 2017). Additionally, land use, especially agriculture, amplified the mobilization and discharge of DSi from the watershed to the studied estuaries. Overall, the potential of estuarine ecosystems to modify the river Si flux is large, but poorly understood.

Sediment records are indispensable to gain longer-term perspectives on Si cycling in coastal ecosystems. Ultimately, we want to be able to disentangle the effects of changing DSi utilization by diatoms, Si recycling rates in the water column and varying sediment deposition rates. This study aims to constrain the Si fluxes from continents to coastal environments by identifying the major processes controlling the Si budget in the CB based on biogenic silica (BSi) accumulation rates and the silicon isotope composition of diatoms ($\delta^{30}Si_{diatom}$) in two sediment cores covering most of the Holocene. Their proximal and distal location relative to the main tributary, the Susquehanna River (Fig. 1), allows us to distinguish terrestrial from oceanic influences on the local Si cycle. High sediment organic matter (OM) and clay contents and low BSi concentrations < 10 wt% make diatom extraction and purification challenging but achievable via hand-picking of individual diatom frustules. Previously published data were used to reconstruct precipitation, nutrient input, diatom assemblages, vegetation patterns and human activity, which provide a comprehensive framework for the interpretation of DSi fluxes in CB sediments (Cooper 1995; Cronin et al. 2005; Kemp et al. 2005; Willard et al. 2015).

In this study we focus on vegetation change—both natural and anthropogenic—as a process perturbing Si cycling within the CB catchment. We hypothesize that $\delta^{30}Si_{diatom}$ varies as a function of catchment vegetation changes and hydrology conditions (including salinity changes and shifts of the main water mixing zone) driven by influences of climate change and/or human activity on $\delta^{30}Si_{diss}$. Proposed processes are summarized in Table 1.

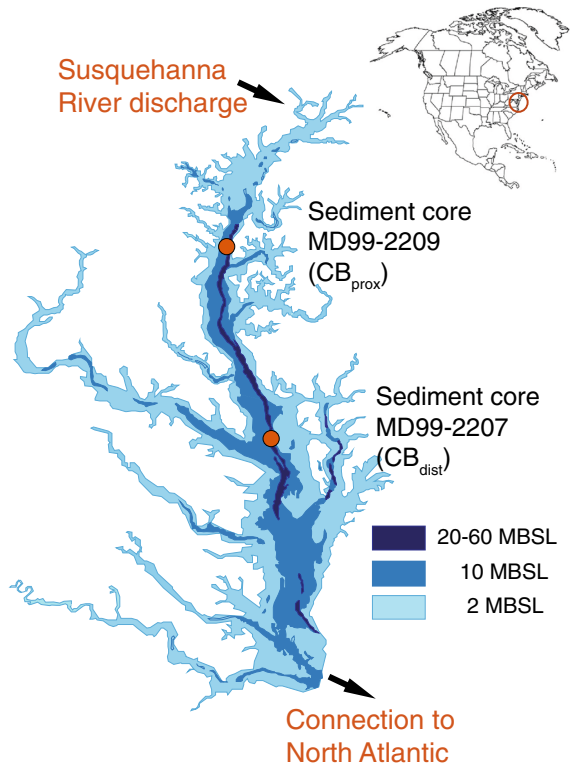

Fig. 1 Chesapeake Bay with locations of sediment cores MD99-2209 (CB_{prox}, 38° 88′ N, 76° 39′ E) and MD99-2207 (CB_{dist}, 38° 03′ 05″ N, 76° 21′ 47″ E) (Cronin et al. 2005)

Study site

The Chesapeake Bay (Fig. 1), located on the East Coast of North America, is a large estuary with a surface area of $\sim$ 11,500 km^2. The majority of the bay is relatively shallow (mean water depth of 8 m), but a deep channel in the center of the CB (up to 60 m water depth) provides a variety of habitats for different kinds of phytoplankton. Its 166,000 km^2 catchment includes numerous tributaries that supply around 60 km^3 a^{-1} freshwater to the bay (D'Elia et al. 1983). Presently, the main tributary—the Susquehanna River—delivers more than 50% of the freshwater and creates brackish conditions (surface salinity < 5‰) in the northern CB (Malone et al. 1996).

Located at the transition zone between the North American continent and the Atlantic Ocean, the CB and its catchment experience large variations in nutrient inputs, sea level, vegetation, precipitation, pH and salinity on seasonal to centennial time scales

(Kemp et al. 2005). Local climate varies with the North Atlantic Oscillation (NAO) (Hurrell 1995), with positive NAO states leading to higher precipitation primarily during winter (Vega et al. 1999; Cronin et al. 2005). Water mixing between freshwater and marine water in the mesohaline center of the CB is important for the distribution of nutrients in the estuary, including Si and N (Brush 2009). Primary production in the low salinity regions of the northern CB is generally limited by light and phosphorus, and transitions to nitrogen limitation in the higher salinity regions of the CB (Malone et al. 1996; Fisher et al. 1999). Phytoplankton blooms in the CB main stem between January and April are dominated by diatoms (~ 56–80%). Main diatom taxa in the modern CB are *Skeletonema costatum* and *Cyclotella* species (Hagy et al. 2005; Marshall et al. 2006). *S. costatum* dominates during the early part of the bloom, while *Cyclotella* grows later in April/May. High primary production leads to nutrient depletion (P and Si) in the mid- and lower- CB at the end of the spring bloom (April/May) (Conley and Malone 1992; Correll et al. 2000; Hagy et al. 2005).

Anoxic/hypoxic bottom waters during summer have been observed in the CB since the 1950s. Oxygen depletion in the mesohaline region during spring and summer relates to freshwater discharges and increased nutrient fluxes of N and P (Hagy et al. 2004).

Holocene development and summary of previous work

The development of the CB since the LGM has been driven by changes in climate, sea level and catchment land use. Eustatic sea level rise of about 14 m between 9500 and 7500 a BP transformed the CB from a fluvial deltaic system into an estuary, altering water chemistry and mixing conditions (Cronin et al. 2007). Periods of increased sediment inputs from the watershed into the CB are connected with two major phases of deforestation between 250 and 50 a BP (Pasternack et al. 2001; Cronin and Vann 2003). A sixfold increase in sediment accumulation associated with land clearance around ~ 250 BP (Colman et al. 2002) reflects a major perturbation to the watershed coincident with European settlement. Increasing eutrophication, documented by N and P concentrations, led to a nearly or completely anoxic condition in the bottom waters during the last ~ 220 years, as indicated by the preservation of laminated sediments in the northern CB (Bratton et al. 2003b).

River discharge into CB is highly dependent on regional precipitation and is therefore connected to local and global climate variations (Cronin et al. 2005). Holocene precipitation estimates, based on paleosalinities inferred from foraminiferal $\delta^{13}C$ and $\delta^{18}O$ (Cronin et al. 2005) suggest drier conditions for the Early Holocene (12000–5900 a BP) and wetter conditions during the later Holocene (5900–250 a BP) (Saenger et al. 2006). Pollen records from the CB watershed demonstrate that catchment vegetation varied during the Holocene and can be used to infer climate and land use changes (Brush 2001). A shift from *Quercus* (oak) to *Pinus* (pine) dominated vegetation around 6000 a BP has been linked to warmer winter temperatures and increased humidity (Willard et al. 2005). Increasing *Ambrosia* assemblages document European settlement and large-scale agriculture in the watershed since around 200 a BP (Willard et al. 2003). The CB watershed simultaneously changes from a forested, freshwater-dominated site to a more open ecosystem influenced by more saline waters (Willard et al. 2005). Given the connections between vegetation, Si (re)cycling and Si export rates from soils outlined above, we expect to see coeval variations in Si cycling.

Holocene diatom assemblages in CB sediments tend to be dominated by the centric species *Cyclotella caspia* and *Cyclotella striata* (Cooper 1995) that are tolerant of changes in environmental conditions like salinity, temperature, water depth and nutrient inputs (Van Dam et al. 1994; Cooper 1995). We found only a few frustules of the more fragile *S. costatum* in the sediment cores. Eutrophication and anoxia over the last 250 years have led to decreased diatom diversity since 1760 and an significant increase in c/p ratio since 1940 (centric (mostly planktonic) to pennate (mostly benthic) diatom ratio) (Cooper and Brush 1993).

Materials and methods

Sediment cores (MD99-2207 and MD99-2209) were retrieved during the MAGES V cruise of the *Marion-Dufresne* in summer 1999 by the U.S. Geological Survey (USGS) using a Calypso piston coring system. Core MD99-2207 (38° 03′ N, 76° 21′ E, water depth:

23.1 m) has a length of 2070 cm and core MD99-2209 (38° 88′ N, 76° 39′ E, water depth: 26.5 m) a length of 1720 cm (Fig. 1) (Colman et al. 2002). Sediment core MD99-2209 (CB_{prox}) is located proximal to the Susquehanna River mouth and therefore predominantly influenced by freshwater discharge (modern salinities between 10 and 12 PSU) (Colman et al. 2002) (Fig. 1). Sediment core MD99-2207 (CB_{dist}) is located distal to the Susquehanna River and is more influenced by saline water (modern salinities between 15 and 18 PSU), due to its vicinity to the Atlantic Ocean (Colman et al. 2002) (Fig. 1).

One cm thick samples were extracted from both sediment cores every 10 cm for the more recent past (CB_{prox}: − 41 to 475 a BP; 10–390 cm; CB_{dist}: − 37 to 3565 a BP; 10–500 cm) and every 20 cm (CB_{prox}: 507–6729 a BP; 400–1600 cm; CB_{dist}: 3942–12,352 a BP; 528–2068 cm) for the remainder of the cores. The temporal resolution of the samples varies between both sediment cores and ranges from 2.5 to 1009 years with a mean of 62 years in CB_{prox} and from 2.3 to 665 years with a mean of 96 years in CB_{dist}. One reason for the large differences are the variable sedimentation rates that range from 0.02 to 1 g cm^{-2} a^{-1} in CB_{prox} and from 0.01 to 0.7 g cm^{-2} a^{-1} in CB_{dist}.

Chronology

The chronologies for both sediment cores are based on previously published ^{210}Pb, ^{137}Cs and calibrated ^{14}C dates measured on mollusks and foraminifers, 29 ^{14}C dates for core CB_{dist} and 25 ^{14}C dates for CB_{prox}, using a reservoir age of 400 years (Cronin et al. 2000, 2003; Colman et al. 2002). Linear interpolation between the available dates was made to generate continuous age models for both sediment cores. All ages are expressed in cal a BP (i.e. years before AD 1950). Samples from sediment core MD99-2207 covers the last ∼ 12400 years and MD99-2209 reaches back to ∼ 7600 a BP. For further details on the chronologies, see Colman et al. (2002).

Diatom preparation and $\delta^{30}Si_{diatom}$ measurements

Diatom frustules were extracted following Morley et al. 2004. About 3 g of dry sediment was treated with 30 ml of 33% H_2O_2 and heated to 50 °C to remove the organic matter. 5 ml of 5% HCl was added to remove any carbonates. Heavy liquid separation using sodium polytungstate at densities of 2.3, 2.2 and 2.1 g cm^{-3} removed the minerogenic fraction. To further separate clays and divide the diatoms into different size fractions, the samples were wet-sieved with 53 µm, 25 µm and 5 µm mesh sizes. After the visual inspection of all grain-size fractions between 300 and 400 centric diatoms from the genus *Cyclotella* were hand-picked from the largest diatom fraction (> 53 µm) using a binocular microscope at 50 × magnification to minimize contamination and potential species dependent fractionation (i.e. "vital-effects") (Sutton et al. 2013). The investigation of only one genus provides consistency in our isotope data reflecting the April/May bloom periods and epilimnic water conditions.

The diatom frustules were dissolved in 0.5 ml 0.4 M NaOH before cation exchange chromatography (Georg et al. 2006) to remove Na and any other cationic contaminants. Analysis of column eluates by ICP-OES did not reveal any contamination, with Si/Na molar ratios always much greater than 25. Al was always below detection limit. The final Si solutions as well as the standards (NBS28, diatomite) were diluted to 0.6 ppm Si in an 0.1 M HCl matrix and doped with 0.6 ppm Mg for mass-spectrometry. $\delta^{30}Si_{diatom}$ was assessed on a Neptune MC-ICP-MS (multi collector inductively coupled plasma mass spectrometer) using matrix-matched sample-standard bracketing at the German Research Centre for Geosciences Potsdam (GFZ) following standard protocols (Oelze et al. 2016).

Mg isotopes were monitored in dynamic mode to correct for instrumental mass bias following (Cardinal et al. 2003). The corrected ratio of ^{30}Si to ^{28}Si is:

$$\left(\frac{^{30}Si}{^{28}Si}\right)_{corr} = \left(\frac{^{30}Si}{^{28}Si}\right)_{meas} \times \left(\frac{^{30}Si_{AM}}{^{28}Si_{AM}}\right)^{f_{Mg}}$$

where $(^{30}Si/^{28}Si)_{meas}$ is the measured value and $(^{30}Si_{AM}/^{28}Si_{AM})$ are the atomic masses of ^{30}Si and ^{28}Si. f_{Mg} was determined using the beam intensities on masses 24 and 26. The Si isotope ratios are given relative to the NBS28 standard. Three individual bracketed measurements (standard-sample-standard) were averaged for $\delta^{30}Si$ and $\delta^{29}Si$, respectively:

$$\delta^{30}Si = \left(\frac{R_{sam}}{R_{std}} - 1\right) \times 1000$$

where R_{sam} and R_{std} are the corrected ratios of ^{29}Si and ^{30}Si to ^{28}Si. Drift of Mg peak for a subset (26) of samples made conventional standard-sample bracketing (SSB) the preferred option to correct for instrumental mass bias. The mean offset between SSB and Mg-corrected + SSB for the 48 other samples was 0.06 ± 0.07‰. Figure 2 shows all 74 $\delta^{30}Si_{diatom}$ samples used in this study in a three-isotope plot $\delta^{29}Si$ vs. $\delta^{30}Si$. The plot indicates the absence of polyatomic interferences during mass spectrometry because all samples fall on the expected mass fractionation line (gradient = 0.5056) (Reynolds et al. 2007). The secondary reference materials, Diatomite and BHVO-2 were prepared and measured throughout the same sessions. Analysis yielded values of 1.25 ± 0.06‰ (n = 10) and − 0.30 ± 0.04‰ (n = 3), respectively (2SD), in line with published values (Reynolds et al. 2007; Savage et al. 2014). Typical internal precisions of all samples were ≤ 0.05‰. In this lab a long-term precision of 0.14‰ (expressed as 2SD) was determined, which we use here as our analytical uncertainty estimate, determined through 133 measurements of reference material BHVO-2 (Oelze et al. 2016). Signal intensities on each of the isotopes resulting from instrumental background and acid blanks were always < 1% of sample intensities.

Biogenic Si

The biogenic silica (BSi) concentration in CB_{dist} and CB_{prox} sediments was determined using a sequential alkaline extraction method (DeMaster 1981; Conley and Schelske 2001). About 30 mg of dried and homogenized sediment material was dissolved in 40 ml of 0.1 M Na_2CO_3 by shaking and heating at 85 °C for 5 h. A 1 ml aliquot was subsampled after 3, 4 and 5 h of reaction and neutralized with 9 ml 0.021 M HCl. The DSi concentrations of all samples (n = 242) were determined colorimetrically with a SmartChem 200 discrete chemical analyzer using the molybdate-blue methodology (Eggimann et al. 1980). Ascorbic acid was used as a reductant. The BSi content was calculated by determining the intercept of a least-squares regression between total extracted Si

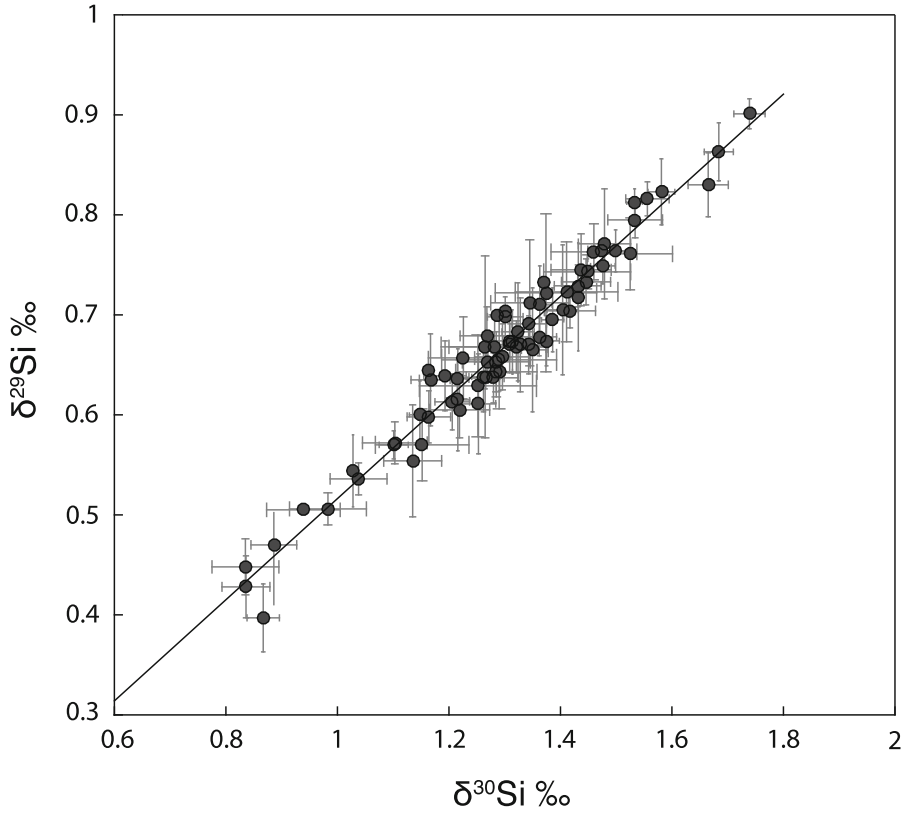

Fig. 2 Three-isotope plot ($\delta^{29}Si$ vs. $\delta^{30}Si$) from CB sediments covering all measured diatom samples from CB_{prox} and CB_{dist}. Errorbars reflect measurement uncertainties (2σ). The solid line indicates the mass fractionation line with a gradient of 0.5

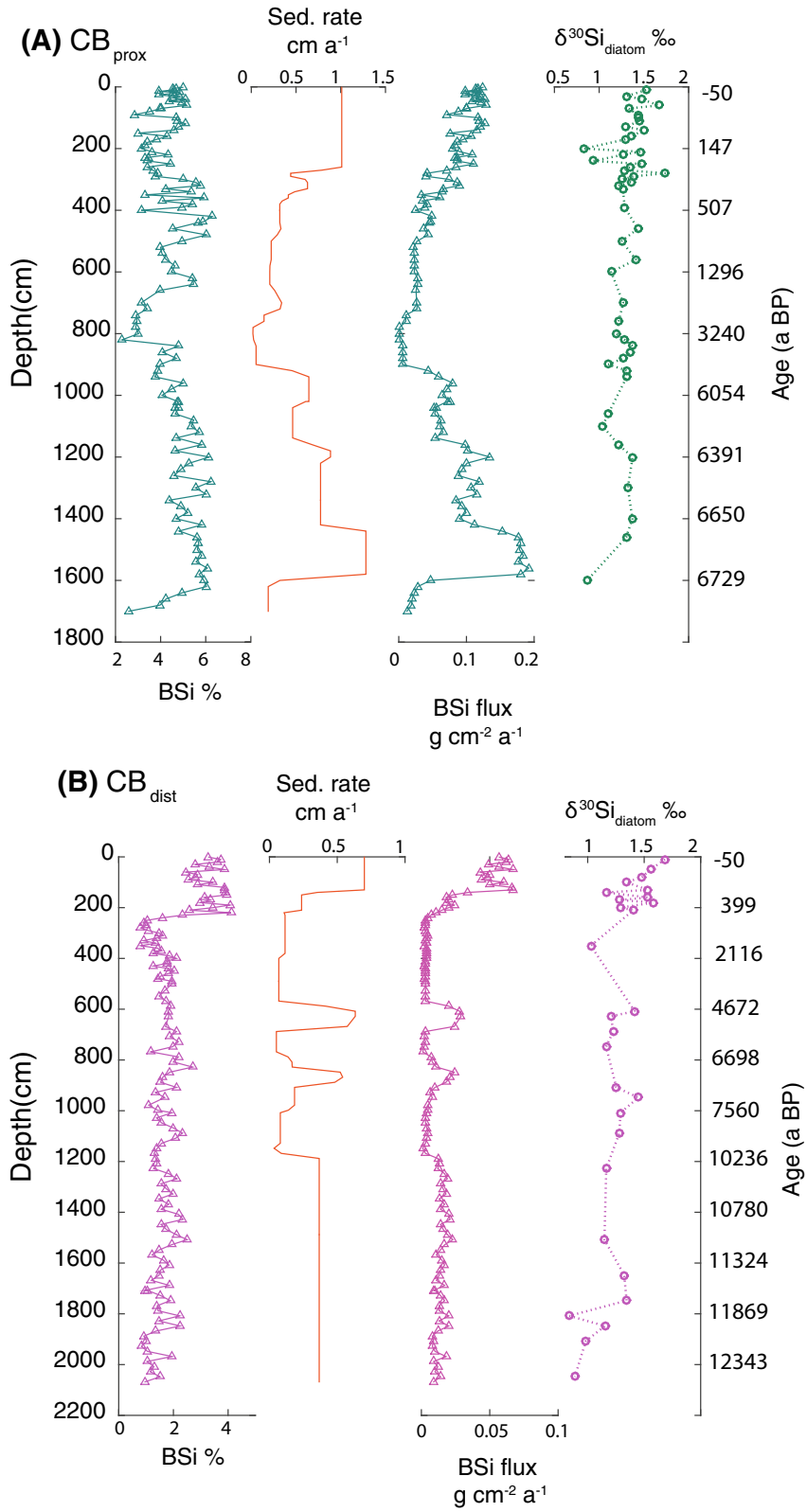

Fig. 3 BSi (%), sedimentation rate (cm a^{-1}), BSi flux (g cm^{-2} a^{-1}) and $\delta^{30}Si_{diatom}$ from sediment core MD99-2209 (CB_{prox}) (**a**) and MD99-2207 (CB_{dist}) (**b**)

and extraction time (Conley 1998; Sauer et al. 2006). Additionally, 87 duplicates were measured (36% of all samples) with an average standard deviation of 0.167 (CB_{prox}: 0.104, CB_{dist}: 0.212).

XRF

The elemental composition of 99 freeze-dried and homogenized sediment samples was determined using a Thermo Scientific Niton XL3t GOLDD + X-ray fluorescence analyser (ThermoFisher Scientific Inc., Waltham, MA, USA) at Lund University, Sweden set to mining mode (Cu/Zn) for 180 s, detecting elements in the range of Na to U. Titanium concentrations (ppm) are presented here to provide additional information on detrital input within the uppermost 400 (CB_{prox}, ~ 507 a BP) and 500 (CB_{dist}, ~ 4324 a BP) cm of both sediment cores, respectively. Calibration of the XRF device was performed against a soil standard reference material (SRM 2709a San Joaquin Soil) (Mackey et al. 2010).

Results

CB_{prox}, $\delta^{30}Si_{diatom}$

$\delta^{30}Si_{diatom}$ in core CB_{prox} varies between 0.84 and 1.74‰, with a mean of 1.31‰ (Fig. 3a). $\delta^{30}Si_{diatom}$ is relatively consistent at ca. 1.2‰, with the exception of low isotope ratios between 900 and 1440 cm sediment depth (~ 5800 and 6700 a BP) and values between 0.87 and 1.01‰ from 540 cm sediment depth (~ 1000 a BP) until the core top. The sediment interval from 290 cm depth upwards (~ 250 a BP) is characterized by the greatest $\delta^{30}Si_{diatom}$ variability, including the minimum and maximum values of the record (Fig. 3a).

CB_{prox}, BSi

BSi concentrations in CB_{prox} vary between 2.29 and 6.28%, around a mean of 4.57% (Fig. 3a). An interval of high BSi concentrations between 1655 and 855 cm sediment depth (~ 7000–5000 a BP) is followed by lower values between 2 and 4% until 600 cm sediment depth (~ 1300 a BP). Greater variability in the uppermost 525 cm (ca. 1000 years) accompanies a higher sampling resolution. The BSi accumulation rate ranges from 0.001 to 0.192 g cm^{-2} a^{-1} with a mean of 0.076 g cm^{-2} a^{-1}. Two maxima in the mid Holocene around 1285 cm (6500 a BP) and between 1440 and 1580 cm sediment depth (6700 and 6725 a BP) reach 0.119 and 0.192 g cm^{-2} a^{-1}, respectively. At 760 cm sediment depth (around 2000 a BP) the BSi flux increases from around 0.006 to between 0.026 and 0.064 g cm^{-2} a^{-1} until 340 cm sediment depth (340 a BP). A further sharp increase towards a BSi flux maximum of 0.129 g cm^{-2} a^{-1} occurs at ~ 60 cm sediment depth (8 a BP, CE 1942) (Fig. 3a).

CB_{dist}, $\delta^{30}Si_{diatom}$

$\delta^{30}Si_{diatom}$ in sediment core CB_{dist} varies between 0.84 and 1.68‰ with a mean of 1.29‰ (Fig. 3b). The Si isotope record is relatively stable through most of the core, with the exceptions of some values < 1‰ between 2048 and 1748 cm sediment depth (12,350–11,720 a BP) and two positive excursions around 950 (1.43‰) and 620 cm (1.50‰) sediment depth (~ 7300 and ~ 4700 a BP). $\delta^{30}Si_{diatom}$ variability with a higher resolution and values between 1.17 and 1.68‰ occurs above 165 cm core depth (~ 250 a BP) (Fig. 3b).

CB_{dist}, BSi

BSi concentrations in CB_{dist} vary between 0.81 and 4.11% around a mean of 1.92%. Relatively stable values throughout the sediment core precede an abrupt increase around 240 cm sediment depth (680 a BP) from 1.03 to 4.11%. The BSi flux varies between 0.001 and 0.067 g cm^{-2} a^{-1}, with a mean flux of 0.015 g cm^{-2} a^{-1}. Three maxima at around 888 (7000 a BP), 565 (4500 a BP) and in the topmost 165 cm (since 250 a BP) can be attributed to changes in total sedimentation rates. A stepwise increase in BSi flux from below 0.004 to 0.024 g cm^{-2} a^{-1} at ~ 180 cm sediment depth (314 a BP) is followed by a second increase to 0.067 g cm^{-2} a^{-1} at 130 cm core depth (~ 134 a BP) (Fig. 3b).

Table 2 Results of the mass balance calculation for the CB based on DSi flux data (D'Elia et al. 1983) and BSi flux data measured in sediment cores MD99-2207 and MD99-2209 in Gmol a^{-1}. Scenarios B to D describe modifications of the basic mass balance considering specific input and output conditions of the CB core locations

				total CB	northern CB
Basic mass balance	A	Input	DSi flux (Gmol a^{-1})	3.23	1.76
		Output	BSi flux (Gmol a^{-1})	10.31	2.68
		BSi deposition %		319	152
+ modified input	B	Input	DSi flux (Gmol a^{-1})	3.23	1.76
			BSi flux (Gmol a^{-1}) 30%	0.97	0.53
		Output	BSi flux (Gmol a^{-1})	10.31	2.68
		BSi deposition %		245	117
	C	Input	DSi flux (Gmol a^{-1})	3.23	1.76
			BSi flux (Gmol a^{-1}) 30%	0.97	0.53
			Groundwater flux (Gmol a^{-1}) 40%	1.29	0.70
		Output	BSi flux (Gmol a^{-1})	10.31	2.68
		BSi deposition %		188	89
+ modified input & output	D	Input	DSi flux (Gmol a^{-1})	3.23	1.76
			BSi flux (Gmol a^{-1}) 30%	0.97	0.53
			Groundwater flux (Gmol a^{-1}) 40%	1.29	0.70
		Output	BSi flux (Gmol a^{-1}) 50 and 75%	5.16	2.01
		BSi deposition %		94	67

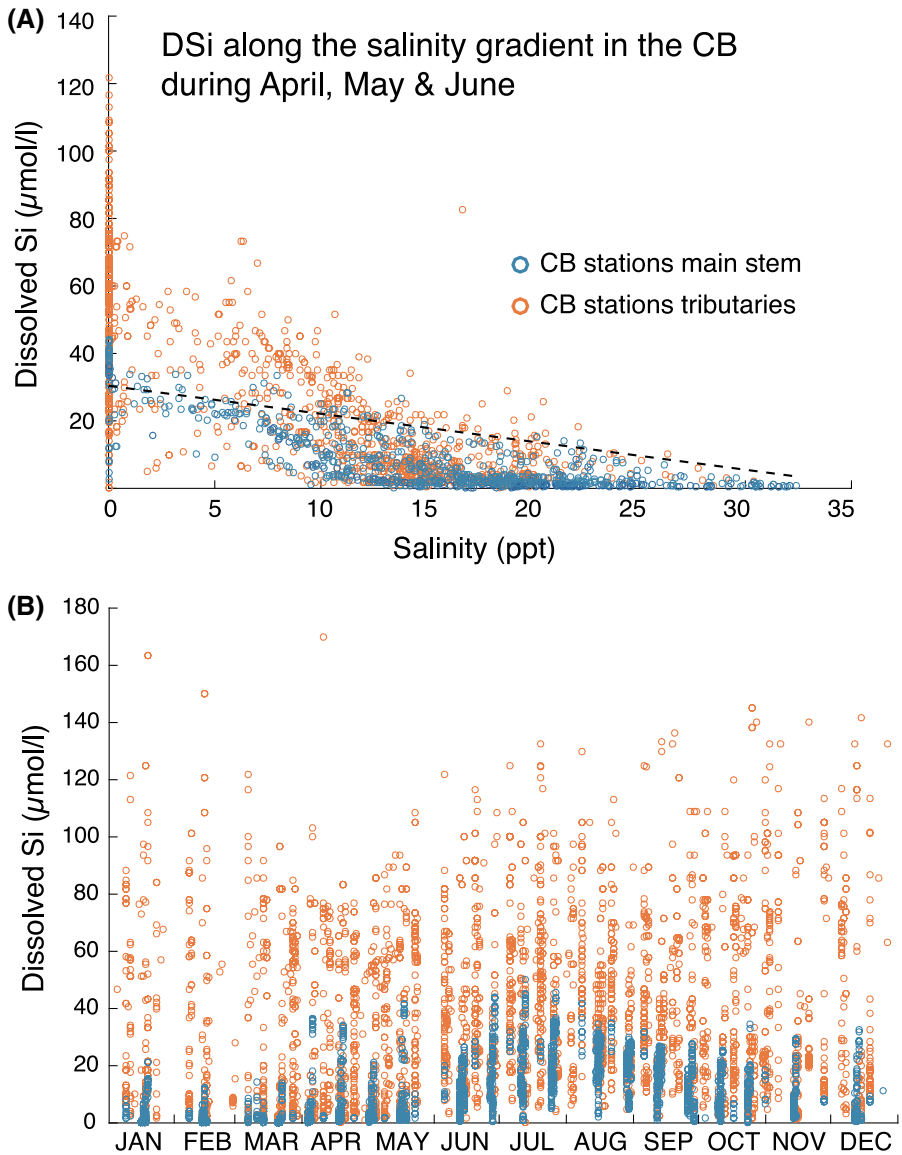

Fig. 4 **a** Dissolved Si plotted against salinity in the Chesapeake Bay during April, May and June 1989 (− 39 a BP). Conservative mixing line (dotted line) using as end members the mean DSi of tributary water entering the bay during the same time-slice and assuming shelf water DSi of ∼ 2 µmol l^{-1} (D'Elia et al. 1983). **b** Dissolved Si plotted over time (year 1989, − 39 a BP). Data from the Chesapeake Bay monitoring program (https://www.chesapeakebay.net/what/downloads/cbpwater_quality_database_1984_present). Orange data points: DSi in tributaries, blue data points: DSi in the CB main stem

Discussion

Mass balance: constraining the Si budget in the modern CB

Si mass balances were calculated for the total CB (surface area: 11500 km^2) and the northern CB (surface area 2300 km^2) (Kemp et al. 2005). These budgets are not intended to serve as a precise calculation, but rather a quantitative estimation of the Si cycle in the modern CB. These two separate calculations serve to illustrate regional characteristics of the bay. Furthermore, the northern CB is fed only by the Susquehanna River, which simplifies the calculation. For the whole estuary, we use DSi fluxes of the main tributaries (Susquehanna River 1.76 Gmol a^{-1}, James River 0.72 Gmol a^{-1}, Potomac River 0.59 Gmol a^{-1}), as measured in CE 1982 (− 32 a BP) by D'Elia et al. (1983) and an average BSi concentration (3.83 wt%) of both sediment cores at a depth of 10 cm (approximately CE 1991 (− 41 a BP) in CB_{prox} and approximately CE 1987 (− 37 a BP) in CB_{dist}). These sediment BSi concentrations are similar to those found by Cornwell et al. (1996) in the middle bay. For just

the northern oligohaline CB, we assumed that the main source of the DSi is the Susquehanna River and use only the BSi concentration from the upper 10 cm of CB_{prox} (Table 2).

The mass accumulation rate (MAR) for the calculation of the BSi fluxes was determined following Ragueneau et al. (2001):

$$J_{acc} = (1 - \phi) \cdot w \cdot S \cdot \mathrm{BSi} \quad (1)$$

where w is the sediment density (2.6 g cm^{-3} (Colman and Bratton 2003), S is the sedimentation rate determined using the age model based on ^{14}C dating of CB_{dist} and CB_{prox}, and Φ is an average sediment porosity of 0.95 (Colman et al. 2002).

The results of the mass balance calculation for the CB estuary are shown in Table 2. In both cases, these simple models suggest that much more Si is buried in CB sediments than enters through rivers (319%; scenario A, Table 2). This is also true when considering the northern CB separately (152%). We can rule out a non-steady state explanation, since the total DSi inventory of CB is less than the annual river flux. This discrepancy, therefore, requires that we either underestimate the Si inputs or overestimate the BSi deposition rate in the CB sediments.

Conley (1997) showed that BSi transported by the Susquehanna River is equivalent to around 30% of the DSi flux. If this fraction is representative of all major CB river inputs, then the burial of BSi as a fraction of total Si inputs decreases to 246% for the whole bay and 117%, for the northern section, respectively (scenario B, Table 2). If we consider that groundwater—a non-negligible flux in the global ocean Si budget—is also important in the CB, this might explain some of the discrepancy (Rahman et al. 2019). As previous studies showed, groundwater contributes an additional maximum 40% of river DSi. Taking this value into account, the burial of BSi relative to total inputs decrease in our model further to 188% in the whole bay and 89%, in the northern bay, respectively (scenario C, Table 2) (Burnett et al. 2007; Niencheski et al. 2007; Georg et al. 2009). In other words, even with conservatively large estimates of the key but unmonitored input fluxes, the supply of Si to CB cannot account for its burial in the sediment.

Alternatively, our burial estimate may be biased towards high values. The shape of the CB, with one deep channel in the center, leads to uneven deposition rates throughout the bay (Adelson et al. 2001). Kemp et al. (2005) present hypsometric curves for the upper, mid and lower bay that demonstrate that the deep channel is only a small fraction of total area. The shape of the bay favors sediment focusing from the slopes into the deep parts. Since both sediment cores come from the deep channel, an overestimation of BSi accumulation rate is possible. Further, anoxic water conditions in the deep channel may increase BSi redissolution during summer (Villnäs et al. 2012; Siipola et al. 2016), however, at the same time less bioturbation would enhance the preservation of diatom frustules in the sediments. Consequently the spatial extrapolation to the whole bay area may cause an

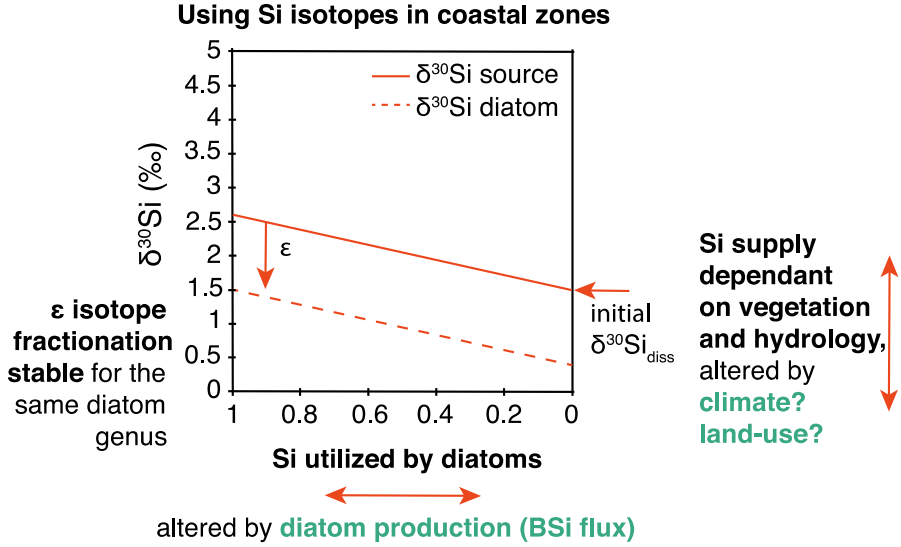

Fig. 5 Steady-state model explaining the influence of $\delta^{30}Si_{diss}$ and BSi flux on the $\delta^{30}Si_{diatom}$ signal in a system with a steady supply of DSi. Edited after Frings et al. (2016). The Rayleigh fractionation model considering a finite pool of reactant is not shown since the difference in $\delta^{30}Si_{diatom}$ is small and therefore negligible

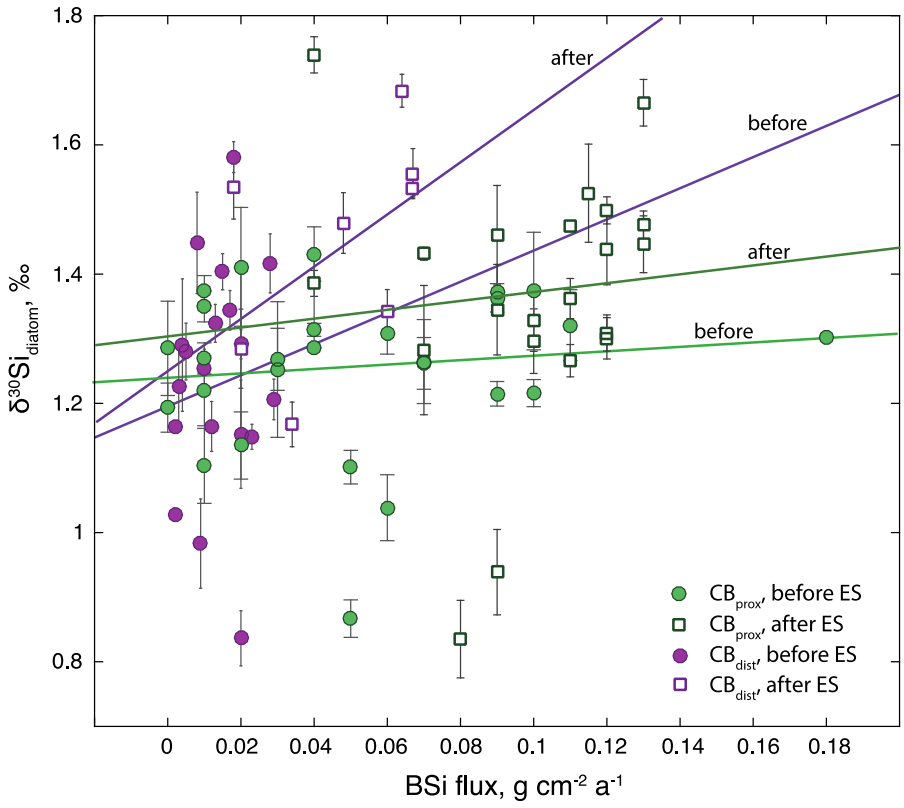

Fig. 6 Correlation-plot: BSi flux plotted against $\delta^{30}Si_{diatom}$ in CB_{dist} (purple markers) and CB_{prox} (green markers). Before European settlement (filled cycles) and after European settlement (open squares). (Color figure online)

overestimation of the calculated BSi flux in the mass balance.

The calculation for the northern CB is further biased by the arbitrary definition of the surface area. It has been shown that due to two layer gravitational circulation, bottom water undercurrents could transport material from the central bay where the maximum production occurs northward, creating the possibility that a part of the BSi in CB_{prox} was produced outside and relocated to northern CB (Hagy et al. 2005). Relatively high sedimentation rates and seasonal anoxic bottom waters, as indicated by banded sediments in CB_{prox}, also favor high diatom preservation rates in the northern CB. To account for these issues the BSi flux in the total and the northern CB the Si output was arbitrarily reduced to 5.16 Gmol a^{-1} (50% reduction) and 2.01 Gmol a^{-1} (75% reduction), respectively in scenario D (Table 2).

Previous studies arrived at an average Si consumption in estuaries of about 20% (calculated global mean) e.g. Amazon River: 50%, Elbe River: 8%, Yangtze River: 10-15%, Red River: 8.5% (DeMaster 2002; Zhang et al. 2007; Luu et al. 2012; Tréguer and De La Rocha 2013; Amann et al. 2014). However, our mass balance model suggests much greater retention efficiency in the CB. Even considering the uncertainties, an estimate of around 90% DSi retention is plausible for CB, and is corroborated by the demonstration of DSi limitation (i.e. complete utilization) in the CB (Correll et al. 2000). This is likely related to the relatively long water residence time of 7.6 months (Dettmann 2001; Du and Shen 2016) compared to other estuaries (e.g. Guadalupe estuary; 1.07 months, Deleware estuary: 3.3 months, all Danish estuaries: < 4 months) (Conley et al. 2000; Dettmann 2001) and thus lower flow velocity favoring relatively high sedimentation rates.

A salinity-concentration plot for CB based on monitoring data (chesapeakebay.net) ($n = 1935$) from April to June 1989 ($-$ 39 a BP), chosen to overlap with the BSi data of the two sediment cores, represents the peak growing season of *Cyclotella* and provides an

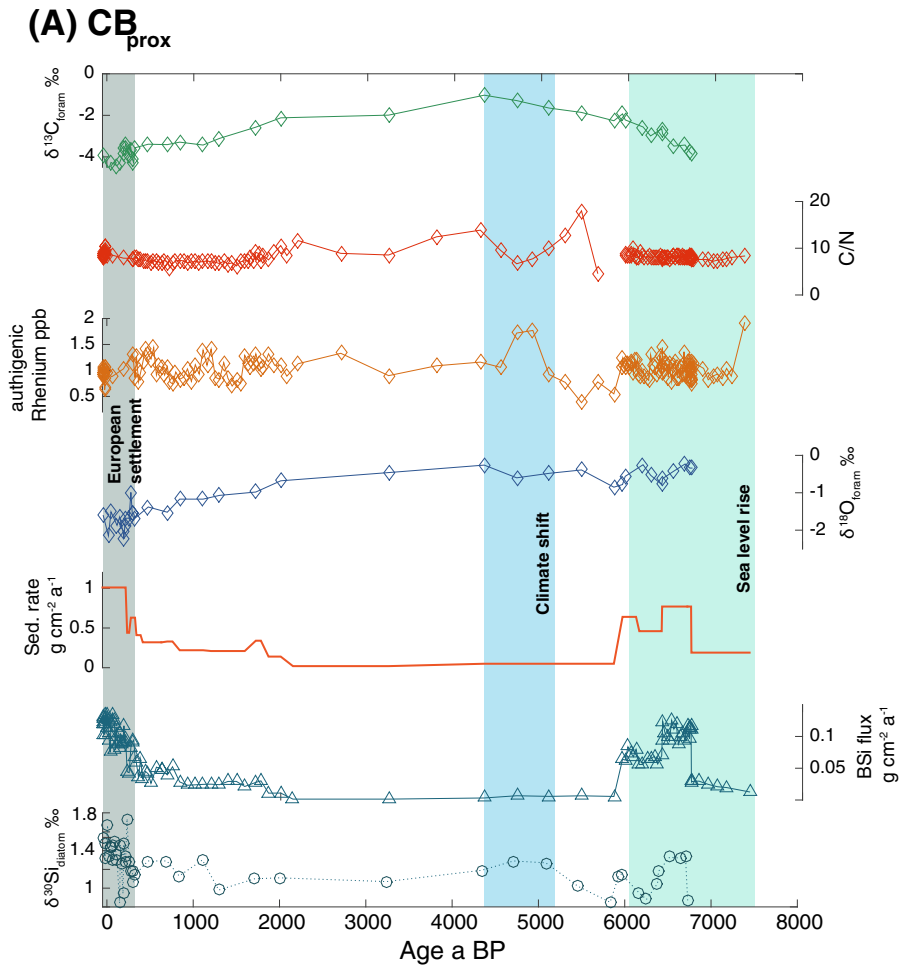

Fig. 7 Compilation of datasets measured on CB_{prox} and CB_{dist} through the Holocene. **a** $\mathbf{CB_{prox}}$: $\delta^{13}C_{foram}$ (Cronin et al. 2005), C/N ratio (Bratton et al. 2003a), authigenic Rhenium (ppb) (Bratton et al. 2003b), $\delta^{18}O_{foram}$ and $\delta^{13}C_{foram}$ (Cronin et al. 2005), sedimentation rate, BSi flux, $\delta^{30}Si_{diatom}$. Pine pollen record (composite from core MD99-2207 and MD99-2209)(Willard et al. 2015). **b** $\mathbf{CB_{dist}}$: $\delta^{13}C_{tot}$ (Bratton et al. 2003a), authigenic Rhenium (Bratton et al. 2003b), C/N ratio (Bratton et al. 2003a), sedimentation rate, BSi flux, $\delta^{30}Si_{diatom}$. The green shaded area indicates the time period of the estuarine development ~ 6000–7600 a BP (Cronin et al. 2007). The blue shaded area indicates a climate shift towards wetter conditions (5000 a BP). The grey shaded area frames the time since European settlement (~ 250 a BP). (Color figure online)

independent line of evidence that Si retention in the CB is high (Fig. 4a). The majority of the samples in the main stem of the estuary (blue data points) fall well below a conservative mixing line (Fig. 4a) indicating active removal. Some samples above the conservative mixing line might indicate re-dissolution of recycled ASi in the water column, or local high DSi river sources. Thus in the main stem most of the remaining DSi is removed during the transport along the salinity gradient of the bay with about ~ 2 µmol l^{-1} remaining in the water column of the southern CB.

Plotted seasonally, the data show that DSi concentrations in the main stem are driven by seasonally varying uptake and supply through the tributaries with low DSi values in winter and spring (Fig. 4b). Low DSi concentrations during the growth period of *Cyclotella* favor the consumption of essentially all available DSi. In this case, $\delta^{30}Si_{diatom}$ must reflect the isotope ratio of the source waters.

A final line of evidence for the near complete removal of DSi in the CB are the relatively high $\delta^{30}Si_{diatom}$ values of 1.53‰ (CB_{prox}) and 1.68‰ (CB_{dist}) in the top of both sediment cores i.e. around 1989 CE. It is commonly assumed that under conditions of complete Si utilization, the diatom silica would reflect the isotopic signature of the source water (river water supplied through tributaries). Supporting this, $\delta^{30}Si_{diatom}$ in both core-tops are in the range of typical river water values (Frings et al. 2016).

Si isotope values measured in diatom frustules from sediments are potentially controlled by three different parameters: the Si isotope composition of the source Si (supplied primarily through rivers and groundwater), DSi utilization by diatoms (reflected by BSi flux to the sediments) and the Si isotope fractionation as DSi is

Fig. 7 continued

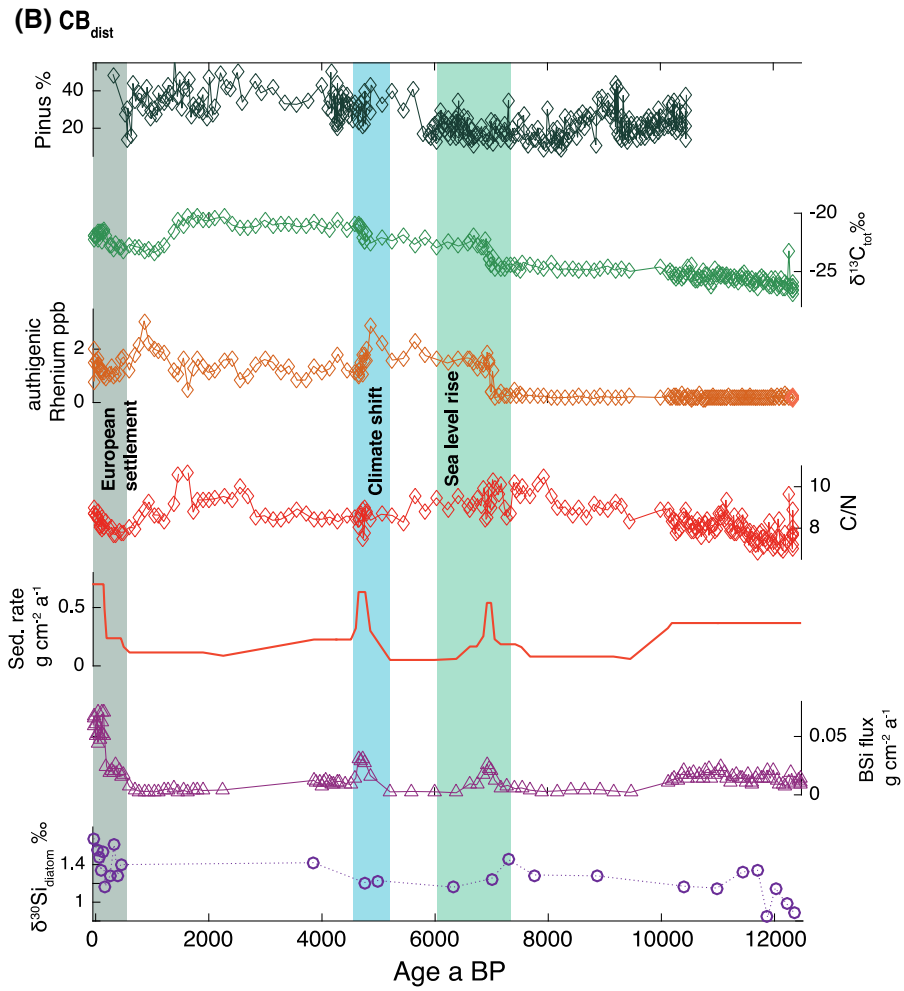

assimilated into the cells. Their influence on the final $\delta^{30}Si_{diatom}$ is shown in Fig. 5, with DSi utilization on the x-axis, initial $\delta^{30}Si_{diss}$ represented by the intercept on the y-axis and the fractionation factor depicted by epsilon (ε). We minimized any effect of species-specific fractionations by hand-picking diatoms from the same diatom genus *Cyclotella*, and therefore assume ε to be constant, albeit uncertain. Thus for the interpretation of our dataset we need only to distinguish between changes in DSi supply and DSi uptake. Since DSi utilization by diatoms can be constrained by our measured BSi fluxes, a positive correlation between $\delta^{30}Si_{diatom}$ and BSi flux would indicate a production-control on the $\delta^{30}Si_{diatom}$ system, i.e. moving along the x-axis of Fig. 5. Diatom production can be altered by ecosystem changes (e.g. salinity, pH, turbidity, N and P availability). In contrast, an absence of correlation between $\delta^{30}Si_{diatom}$ and BSi flux would imply that $\delta^{30}Si_{diatom}$ is to first-order controlled by the Si sources e.g. river $\delta^{30}Si_{diss}$, moving the y-axis intercept of Fig. 5. Two processes in particular have the potential to change the magnitude and/or isotopic composition of the supplied DSi brought into the CB: climate shifts (e.g. more precipitation might increase the DSi supply) and vegetation changes (changes in terrestrial Si cycling influences the $\delta^{30}Si_{diss}$). To distinguish the different Si sources is, however, challenging since there is not yet a proxy for $\delta^{30}Si_{diss}$.

In the following section, we will analyze the variations in Si fluxes in the CB during the Holocene to link BSi accumulation rates and isotope ratios to environmental processes.

Long-term variability (Holocene)

Influence of climate variability between 12400 and 5000 a BP

It is assumed that nutrient fluxes are influenced by climate (Meybeck and Vörösmarty 2005). In the CB changes in Si cycling during the Holocene coincide with sea level rise and vegetation shifts, supporting this hypothesis (Fig. 7a, b). Since our $\delta^{30}Si_{diatom}$ shows only a weak correlation ($r^2 = 0.2$, $p = 0.02$) with diatom productivity (BSi flux) (Fig. 6) we infer that the influence of the river DSi flux must have had a significant influence on the Si cycle in the CB.

Pollen data published for both CB sediment cores imply a forested landscape dominated by *Quercus* und *Pinus* in the Early- and Mid-Holocene (Willard et al. 2005). Ragweed and herb pollen appear at the time of European settlement around 1700 CE (Brush 2009). In general, the pre-anthropogenic forested landscape in the CB catchment would have favored efficient Si recycling rates at the vegetation-soil interface driven by large uptake rates of DSi from the soils and a release of Si from decaying plants. Enhanced decaying of plants releases light ^{28}Si back to the soil and results in an ASi pool with a relatively light $\delta^{30}Si$ composition (Cornelis et al. 2010; Struyf et al. 2010; Vandevenne et al. 2015). By implication the river Si fluxes would be lower in magnitude and lighter in $\delta^{30}Si_{diss}$.

$\delta^{30}Si_{diatom}$ in CB_{dist} indicates an impact of fresh- and marine water mixing on $\delta^{30}Si_{diss}$ in the mesohaline zone. Low $\delta^{30}Si_{diatom}$ (0.8–1‰) in the early Holocene can be explained by greater-than-modern river discharge driven by meltwater generation from the residual Laurentide ice-sheet (Willard et al. 2005). The enhanced freshwater delivery would lead to an increase in DSi flux to the CB, since discharge is among the key drivers of silicate weathering rates (Bluth and Kump 1994; Maher and Chamberlain 2014) and relatively more light DSi available for diatom utilization. A lighter $\delta^{30}Si_{diatom}$ would be the consequence (Cornelis et al. 2010). The increased BSi flux corroborates the larger river Si discharge during the early Holocene. The lack of correlation between diatom production and $\delta^{30}Si_{diatom}$ shows the importance of $\delta^{30}Si_{diss}$ during that time.

Shortly after sea level rise in the CB the Si cycle changes. The BSi accumulation rate in both sediment cores increases between 7000 and 6000 a BP, in particular in CB_{prox}. This is probably linked to additional nutrient supply (Si and N) from the newly inundated areas (Fig. 7a). One would also expect an enhanced residence time as the volume of the bay increased, and thus less horizontal advection of autochthonous BSi. The outcome could be greater preservation of diatom frustules within the bay, favored by slower flow-rates, less turbulence and increasing water depth. Subsequently, maxima in sedimentation rates are visible in both sediment cores. Low $\delta^{13}C_{foram}$ values from this time have been interpreted as indicating terrestrial C as the main carbon source in CB_{prox} (Fig. 7a) (Cronin et al. 2005). However, it is conspicuous that after the period of ecosystem change due to sea level rise, the BSi flux returns to pre-event levels. This may be related to DSi limitation and/or competition with other phytoplankton groups, since the productivity as evidenced by $\delta^{13}C_{tot}$ remains high in both sediment cores (Bratton et al. 2003a). C/N ratios between 7 and 9 at both core locations are relatively stable and suggest marine based carbon as the dominant source, pointing to high phytoplankton productivity (Kaushal and Binford 1999; Meyers and Lallier-Verges 1999) (Fig. 7a, b).

Differences between CB_{prox} and CB_{dist} are probably related to local processes. The proximity to the Susquehanna River of CB_{prox} implicates higher runoff and nutrient supplies favoring productivity. Therefore, any changes in salinity in the Early Holocene are generally small and not recorded in the sediment. The authigenic rhenium (Re) content, a proxy for salinity, is relatively stable (Fig. 7a). Salinity at the distal core location, however, increases abruptly around 7000 a BP, coincident with enhanced productivity (higher $\delta^{13}C_{tot}$), which has previously been linked to increased nutrient supply into the CB from the newly inundated areas (Fig. 7b) (Bratton et al. 2003b). The increase in sedimentary Re concentrations corroborate the growing influence of saline waters at CB_{dist} following sea level rise, since Re is a conservative trace element in seawater with varying concentrations along the salinity gradient (Bratton et al. 2003b). A shift of $\delta^{13}C_{tot}$ to values > -22‰ (Fig. 7b) at the same time implies increasing productivity in the mesohaline region. Simultaneously low variation in $\delta^{30}Si_{diatom}$ implies that diatom productivity is not driving Si cycling in the CB at that time. In a production controlled system the Si isotopes would correlate with the BSi flux. The simplest interpretation of the lack of correlation

between $\delta^{30}Si_{diatom}$ and BSi flux would be complete conversion of DSi by the diatoms. However, changes in the water source (inferred by increasing Re amounts in CB_{dist} (Fig. 7b) mean we cannot rule out that the $\delta^{30}Si_{diss}$ composition changed at the same time, which could act to neutralize any effect of increased diatom productivity on the frustule Si isotope ratio. Greater influence of marine waters, with relatively high $\delta^{30}Si_{diss}$, could be overprinted by the release of Si enriched in relatively light isotopes from the newly flooded shoreline. The increased DSi utilization by diatoms in the northern CB would further lead to an increase of $\delta^{30}Si_{diss}$ at location CB_{dist}. Superimposing processes like precipitation, vegetation and water-mixing conditions drive the Si isotope signal in different directions and could reduce the individual effects of diatom production and varying DSi supply on the $\delta^{30}Si_{diatom}$ and lead to a relatively stable signal (Table 1).

Enhanced BSi fluxes between 6800 and 6000 a BP indicate increased diatom production correlated with higher sedimentation rates. Two minima in $\delta^{30}Si_{diatom}$ (0.8–0.9‰) could be caused by the release of relatively light Si from an additional Si source. Possible sources could include the amorphous Si (ASi) from soil pools in the newly-inundated watershed and ASi stored in plants (phytoliths), both characterized by lighter isotopic signatures (Frings et al. 2016). An increased supply of relatively light Si in DSi fluxes would change the $\delta^{30}Si_{diss}$ in the bay water and consequently in the diatoms.

It has been shown that increased export of DSi from soil pools preferentially releases ^{28}Si and lowers the $\delta^{30}Si_{diss}$ of soil water in a terrestrial ecosystem (Vandevenne et al. 2015). Locally enhanced erosion in near-shore parts of the catchment due to sea level rise and subsequent flooding could lead to the release of Si stored in these pools. Additionally, a decrease in secondary mineral formation rates would lead to a lighter $\delta^{30}Si_{diss}$ signal since clay mineral formation preferentially incorporates the lighter ^{28}Si isotope though the magnitude of fractionation and its manifestation both depend on clay mineralogy, which itself reflects parent lithology, temperature, soil desilication (Si depletion) and hydrology (Opfergelt et al. 2012).

It is perhaps surprising that there is no major difference in the $\delta^{30}Si_{diatom}$ signal before and after sea level rise (Fig. 7b). Changes in salinity—which would have been particularly pronounced at the location of CB_{dist}—might be expected to result in distinct $\delta^{30}Si_{diatom}$ changes. Superimposing processes and Si sources could minimize this effect on the isotope record. Enhanced transport of BSi from the northern CB to the distal core site for example could modify the isotope record at CB_{dist}. Very low BSi concentrations ($\leq 2\%$) in parts of the sediment cores prohibited the measurement of Si isotopes and make this question challenging to answer.

Climate shift $\sim$ 5000 a BP

A composite pollen record for sediment cores CB_{prox} and CB_{dist} (Fig. 7b) shows a doubling of pine pollen abundance in the CB watershed between 5500 and 4800 a BP (Willard et al. 2005). This was linked to increasing winter temperatures and wetter conditions since $\sim$ 6000 a BP. Decreasing Re concentrations and simultaneously increasing $\delta^{13}C_{tot}$ in CB_{dist} indicate decreasing salinities (i.e. greater river runoff) and increasing productivity, supporting the interpretation of a shift towards wetter conditions (Fig. 7b). We observe a peak in BSi flux (around 4700 a BP) while $\delta^{30}Si_{diatom}$ is relatively stable. Increased precipitation and an enhanced freshwater runoff could have led to additional DSi inputs at that time. Previous work suggested that an increase in river flux would lead to a decreased $\delta^{30}Si_{diss}$ (Ding et al. 2004). At the same time, increased diatom production would drive the isotope signal towards heavier values (Fig. 5), counterbalancing a lowering of river $\delta^{30}Si_{diss}$ and explaining the relative stasis of the record. The hand-picked *Cyclotella* diatoms represent late spring/early summer production after the main spring bloom. At that time river runoff might have been smaller compared to early spring, where maximum river runoff creates large DSi fluxes (Fig. 4b). Further, diatoms starting to bloom in January have already diminished the DSi concentration in the main stem of CB (Fig. 4b) (Hagy et al. 2005). The superposition of increased DSi delivery and an enhanced diatom production could explain the constant Si isotope record in CB_{dist} (Fig. 5).

Another possible influence for an increased Si flux could be land use changes in the watershed. A decline of *Poaceae* (grasses) and *Tsuga* (Hemlock, conifer tree) around 5000 a BP points to human influence on vegetation patterns even before European settlement (Willard et al. 2005). Nevertheless, there is no

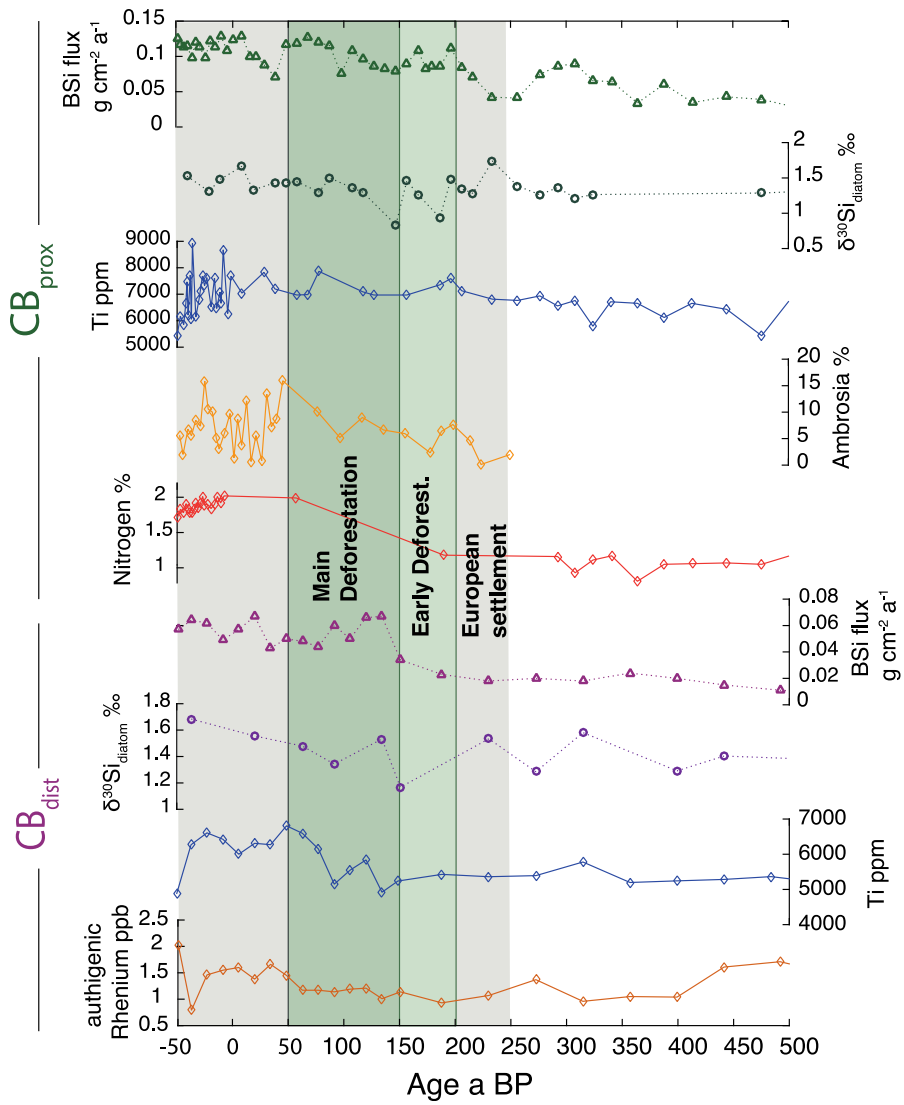

Fig. 8 Variation in $\delta^{30}Si$ and BSi from sediment cores CB_{dist} and CB_{prox} over the last 550 years compared with proxy data sets measured on the same sediment cores. **CB_{prox}**: BSi flux, $\delta^{30}Si_{diatom}$, Ti, Ambrosia pollen (Willard et al. 2003) and nitrogen concentrations (Brush 2009). **CB_{dist}**: BSi flux, $\delta^{30}Si_{diatom}$, Ti and authigenic Rhenium (Bratton et al. 2003b). Green shaded columns indicate deforestation periods in the Chesapeake Bay watershed (Pasternack et al. 2001). Gray shadings reflect human impact in the CB watershed indicated by increasing Ambrosia pollen concentrations. (Color figure online)

indication for changes in Si cycling in the proximal sediment core around that time. The BSi isotope record, as well as the BSi flux remain stable between 5000 and 6000 a BP. One explanation could be the location of CB_{prox}: high river runoff and the dominance of freshwater discharge throughout the year could superimpose small changes in Si isotope composition. In contrast, generally low BSi concentrations in the mesohaline area south of the mixing zone increase around 4700 a BP. Higher DSi input caused by increased land use and erosion in the watershed could lead to enhanced diatom productivity only in CB_{dist}. If we assume that the location of CB_{prox} always was Si replete, we wouldn't see any change here.

To summarize, our results show that sea level rise between 8000 and 7000 a BP influenced the Si budget in the CB reflected by increased BSi production. However, the duration and intensity of this impact is related to the main source of the nutrient. Since CB_{prox} is closely linked to the terrestrial ecosystem through river runoff and groundwater fluxes the change in the Si budget is higher than in CB_{dist}. There, ocean water with a more constant isotope signal (De La Rocha et al. 2000) and a low DSi concentration potentially buffers the influence of short term changes in terrestrial Si fluxes. However, ecosystem shifts driven by water mixing (marine vs. freshwater) modifying the Si budget are only visible in the distal sediment core.

Short-term variability and human impacts since European settlement

Land use changes linked to human activity have been shown to influence the continental Si cycle (e.g. Struyf et al. 2010). We hypothesize a visible impact on the coastal Si budget in CB sediments caused by humans changing Si cycling within the catchment. Our results show that the $\delta^{30}Si_{diatom}$ has varied between 0.84 and 1.74 (CB_{prox}) and 1.17 and 1.68‰ (CB_{dist}) during the last ~ 500 years. Since there is no unambiguous correlation ($r^2 = 0.2$, $p = 0.02$) of $\delta^{30}Si_{diatom}$ with diatom productivity (Fig. 6) additional processes besides diatom production must control the $\delta^{30}Si_{diatom}$ values in the CB (Table 1).

Previous studies have shown the impact of land use changes since European settlement (~ 250 a BP) on the CB estuary. Low $\delta^{13}C_{foram}$ and $\delta^{18}O_{foram}$ reflect enhanced freshwater and C fluxes in the northern CB caused by increased terrestrial inputs from the watershed (Cronin et al. 2005) (Fig. 7). Eutrophication caused a decrease in diatom diversity and an increase in the ratio of centric (mostly planktonic) diatoms to pennate (mostly benthic) species (Cooper 1995) due to spreading anoxia and habitat loss (Kemp et al. 2005). Ragweed pollen (*Ambrosia*) horizons in both CB sediment cores supports the expansion of agriculture after 200 a BP (Willard et al. 2005). Simultaneously, the vegetation in some nearshore regions of the watershed shifts to a species composition typical for brackish marsh conditions, suggesting an increasing influence of saline waters either due to human impact (channelization, damming, land use) or greater inflow of ocean water from the Atlantic (Willard et al. 2015).

Two periods of widespread deforestation in the CB watershed around 200 and 50 a BP are linked to an increased sedimentation rate recorded in both sediment cores (Fig. 8) (Pasternack et al. 2001; Colman et al. 2002). The BSi fluxes begin to increase at the same time (Fig. 8). In CB_{dist} an abrupt increase in BSi content coincides with a period of major deforestation and intensive urbanization since around 150 a BP (Pasternack et al. 2001). A more gradual increase of the BSi flux in CB_{prox} starts slightly earlier ~ 200 a BP and correlates with higher nitrogen fluxes in the northern CB (Fig. 8). Enhanced terrestrial runoff rates together with increased nutrient inputs (preferentially P, N and Si) would favor higher productivity in CB, corroborated by increased $\delta^{13}C_{tot}$ for CB_{dist} and $\delta^{13}C_{foram}$ for CB_{prox} (Fig. 7a, b). A distinct increase in C/N ratios (Bratton et al. 2003a) in CB_{prox} with a maximum of 14.7 around 80 a BP (Fig. 7a) correlates with the major deforestation phase in the CB catchment supporting the idea of increased terrestrial runoff.

Two minima in $\delta^{30}Si_{diatom}$ in CB_{prox} (around 175 and 150 a BP, Fig. 8) coincide with the onset of the deforestation periods in the watershed. Because the diatom production remains relatively high, a change in $\delta^{30}Si_{diss}$ has to be considered as the triggering mechanism. As discussed above, low $\delta^{30}Si_{diatom}$ values could be the result of an additional Si source. One possible scenario would be enhanced ^{28}Si release from belowground soil pools due to depletion of the soil ASi pool after deforestation. This interpretation is supported by greater DSi export in streams draining experimentally deforested ecosystems (e.g. Hubbard Brook) (Conley et al. 2008).

Today, the mesohaline zone of the CB (location of CB_{dist}) tends to be depleted in DSi during the summer months reflecting diatom uptake after the main bloom during the winter/spring (Conley and Malone 1992). The increase in BSi flux 150–200 a BP after early deforestation can be interpreted as an increase in nutrient delivery into the mesohaline zone (Fig. 8), and, perhaps even a shift from a P limited to a DSi limited system (Carey and Fulweiler 2012). Enhanced P inputs and recycling would increase the primary productivity and favor diatom blooms until DSi becomes the limiting nutrient (Kemp et al. 2005).

$\delta^{30}Si_{diatom}$ values vary between 1.17 and 1.68‰ and are not linked to the BSi flux (Figs. 6 and 8). Again, that indicates the influence of a process acting to change the freshwater end-member. Salinity is constant since 500 a BP (shown by authigenic Re, Fig. 8) but Ti concentrations measured on the same sediment core suggest increasing detrital input since ~ 130 a BP (Fig. 8). Higher BSi fluxes, enhanced Ti inputs and a trend towards heavier $\delta^{30}Si_{diatom}$ might reflect a causal relationship: increased runoff leads to enhanced diatom production and a heavier $\delta^{30}Si_{diatom}$ signal. Moreover, low $\delta^{30}Si_{diatom}$ values are probably caused by an additional Si source. As with the periods of deforestation, possible sources include the relatively light Si from soil pools and/or enhanced groundwater discharge.

An overall increasing trend in diatom Si isotope ratios in the CB since European settlement likely

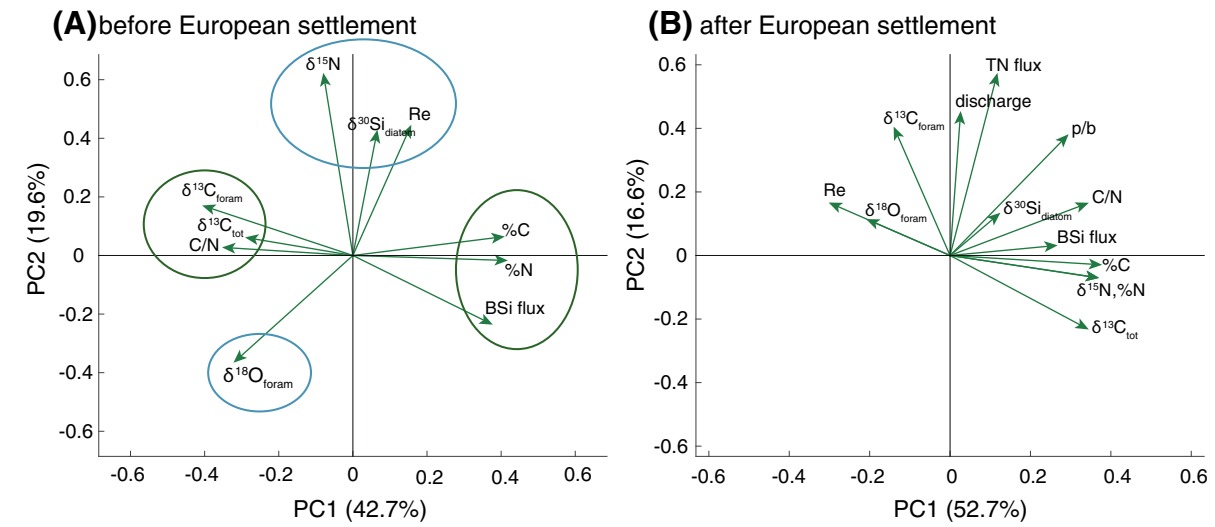

Fig. 9 Principal component analysis of CB_{prox} **a** before European settlement and **b** after European settlement. $\delta^{15}N$, %N, %C, TN flux (Bratton et al. 2003a), $\delta^{13}C_{tot}$, Re (Bratton et al. 2003b), $\delta^{13}C_{foram}$, $\delta^{18}O_{foram}$ (Cronin et al. 2005), discharge (Susquehanna River) (Saenger et al. 2006), p/b ratio (Cooper 1995)

reflects several processes acting in concert, including diatom production, crop harvesting and damming of tributaries, which all act to shift $\delta^{30}Si_{diatom}$ towards higher values (Fig. 8, Table 1). In addition, due to its proximity to the main tributary CB_{prox} seems to be more directly sensitive to changes in the watershed. Stronger stratification and more anoxic conditions in the northern CB (indicated by banded sediment deposition in the topmost ~ 3 meters of the core (the last ~ 270 a BP) would favor higher diatom preservation rates in the sediment due to less bioturbation.

Diatom Si isotope ratios and BSi fluxes are uncorrelated indicating complex processes controlling the Si budget in CB in the last 2000 years. CB_{prox} is directly influenced by Susquehanna River discharge, so more likely records changes of Si cycling in the watershed than CB_{dist}. In contrast, the increase in BSi flux coincident with deforestation during European settlement (150 a BP) in CB_{dist}, indicates a shift from a nutrient limited to a nutrient replete environment for diatoms caused by greater sediment supply.

Processes controlling the Si cycle before and after European settlement

Our results indicate the influence of human activity on Si cycling in the CB. To test the effects of the underlying processes, we compare our data before and after European settlement. Figure 6 shows measured $\delta^{30}Si_{diatom}$ values against BSi fluxes. There is no significant correlation between BSi flux and isotope values either before or after European settlement. As discussed above, this result implies that diatom production is not the dominant control on $\delta^{30}Si_{diatom}$, and instead requires a changing $\delta^{30}Si_{diss}$. In the following we evaluate if these processes are different before and after the period of increased human activity since ~ 250 a BP.

Compiling a variety of proxy datasets in a principle component analysis (PCA) shows different processes potentially controlling our measured $\delta^{30}Si_{diatom}$ before and after European settlement in the northern CB (Fig. 9). Before European settlement (Fig. 9a) $\delta^{30}Si_{diatom}$ plots with authigenic Re and ^{15}N on the second axis, both reflecting changes in water masses and terrestrial input into the bay (19.6% explained total variance), while sedimentary BSi flux lies uncorrelated on the first axis (42.7% explained total variance). These correspondences suggest that Si cycling before

the major human perturbations is controlled by Si and nutrient delivery into CB, rather than by DSi utilization through diatoms. Consequently, large amounts of Si reaching CB from the continent might have remained mobile and transported into the ocean.

In contrast, after European settlement (Fig. 9b) $\delta^{30}Si_{diatom}$ depicts a strong covariance with BSi flux and planktonic to benthic diatom ratio (p/b), proxies of diatom productivity, while the input proxies Re and $\delta^{18}O$ appear uncorrelated with $\delta^{30}Si_{diatom}$. This can be interpreted in terms of enhanced Si utilization and deposition in CB sediments during times of enhanced diatom productivity. Efficient drawdown of DSi by diatoms have strengthened the filter capacity of CB and led to a reduced Si flux into the ocean, as suggested above by our mass balance calculation of the modern CB. However, coastal ecosystems are very diverse, and future work could assess how representative the Holocene development of the CB is relative to the behavior in other coastal ecosystems.

Conclusions

The investigation of two sediment cores from the main stem of the Chesapeake Bay illustrates the importance of coastal zones in the global Si cycle. Our results identify potential processes that can modify the magnitude and isotope composition of Si fluxes between the terrestrial and the oceanic Si cycles.

The modern Si cycle in the Chesapeake Bay appears to be dominated by DSi consumption through diatom production in spring/summer, which is responsible for retaining the majority of Si supplied by its tributaries. Through the Holocene, Si cycling in the CB is sensitive to changes in sedimentation rate due to both climatic change (i.e. sea level rise $\sim$ 7000 a BP, higher runoff since 2000 a BP) and human impact (i.e. deforestation since $\sim$ 250 a BP). Low $^{30}Si/^{28}Si$ isotope ratios in the sediment core most proximal to the Susquehanna River (CB_{prox}) indicate the supply of relatively low $\delta^{30}Si$ to the CB during periods of increased erosion linked to deforestation. Local influences alter $\delta^{30}Si_{diatom}$ at each sediment core location, with potential parameters including freshwater and seawater mixing ratios, bottom water oxygenation affecting preservation, erosion rates, river runoff and net DSi supply.

As a hotspot of anthropogenic influence and lying at the interface of the terrestrial and marine Si cycles, an understanding of coastal zones is crucial to better understand both the natural and the anthropogenically altered Si cycles. However, competing processes, linked to climate variations (e.g. precipitation, vegetation, or sea level changes) or human activity (e.g. agriculture, damming or eutrophication) can be difficult to disentangle in complex estuarine systems. The mechanisms modifying the land-to-ocean Si fluxes might be further elucidated by investigations in less complex settings.

Acknowledgements Open access funding provided by Lund University. We thank Steve Coleman and Debra Willard for providing samples from sediment cores MD99-2207 and MD99-2209. Special thanks also to Brian Buczkowski for subsampling the topmost meters of both sediment cores. Funding from the Kunglig Fysiografiska Sällskapet in Lund (Sweden) supported the preparation and measurement of the samples used in this publication. This work was also partially supported by the Swedish Research Council (VR) to Daniel J. Conley. Markus Czymzik was financed by a German Research Foundation Grant (CZ 227/4-1).

References

Adelson JM, Helz GR, Miller CV (2001) Reconstructing the rise of recent coastal anoxia; molybdenum in Chesapeake Bay sediments. Geochim Cosmochim Acta 65:237–252. https://doi.org/10.1016/S0016-7037(00)00539-1

Aller RC (2014) sedimentary diagenesis, depositional environments, and benthic fluxes. Treatise on geochemistry, 2nd edn. Elsevier Ltd., Amsterdam, pp 293–334

Amann T, Weiss A, Hartmann J (2014) Silica fluxes in the inner Elbe Estuary, Germany. Estuar Coasts 38:192–210. https://doi.org/10.1007/s12237-014-9785-6

Barão L, Vandevenne F, Clymans W et al (2015) Alkaline-extractable silicon from land to ocean: a challenge for biogenic silicon determination. Limnol Oceanogr Methods 13:329–344. https://doi.org/10.1002/lom3.10028

Berner RA (1992) Weathering, plants, and the long-term carbon cycle. Geochim Cosmochim Acta 56:3225–3231. https://doi.org/10.1016/0016-7037(92)90300-8

Beusen AHW, Bouwman AF, Dürr HH et al (2009) Global patterns of dissolved silica export to the coastal zone:

results from a spatially explicit global model. Global Biogeochem Cycles 23:1–13. https://doi.org/10.1029/2008GB003281

Bluth GJS, Kump LR (1994) Lithologic and climatologic controls of river chemistry. Geochim Cosmochim Acta 58:2341–2359

Bratton JF, Colman SM, Seal RR (2003a) Eutrophication and carbon sources in Chesapeake Bay over the last 2700 year: human impacts in context. Geochim Cosmochim Acta 67:3385–3402. https://doi.org/10.1016/S0016-7037(03)00131-5

Bratton JF, Colman SM, Thieler ER, Seal RR (2003b) Birth of the modern Chesapeake Bay estuary between 7.4 and 8.2 ka and implications for global sea-level rise. Geo-Marine Lett 22:188–197. https://doi.org/10.1007/s00367-002-0112-z

Brush GS (2001) Natural and anthropogenic changes in Chesapeake Bay during the last 1000 years. Hum Ecol Risk Assess 7:1283–1296. https://doi.org/10.1080/20018091095005

Brush GS (2009) Historical land use, nitrogen, and coastal eutrophication: a paleoecological perspective. Estuar Coasts 32:18–28. https://doi.org/10.1007/s12237-008-9106-z

Burnett WC, Wattayakorn G, Taniguchi M et al (2007) Groundwater-derived nutrient inputs to the upper Gulf of Thailand. Cont Shelf Res 27:176–190. https://doi.org/10.1016/j.csr.2006.09.006

Cardinal D, Alleman LY, de Jong J et al (2003) Isotopic composition of silicon measured by multicollector plasma source mass spectrometry in dry plasma mode. J Anal At Spectrom 18:213–218. https://doi.org/10.1039/b210109b

Carey JC, Fulweiler RW (2012) The terrestrial silica pump. PLoS ONE 7:e52932. https://doi.org/10.1371/journal.pone.0052932

Chou L, Wollast R (2006) Estuarine silicon dynamics. In: Ittekkot V, Unger D, Humborg C, Tac An N (eds) The Silicon Cycle: Human Perturbations and Impacts on Aquatic Systems. Island Press, pp 93–120

Clymans W, Struyf E, Govers G et al (2011) Anthropogenic impact on amorphous silica pools in temperate soils. Biogeosciences 8:2281–2293. https://doi.org/10.5194/bg-8-2281-2011

Colman SM, Bratton JF (2003) Anthropogenically induced changes in sediment and biogenic silica fluxes in Chesapeake Bay. Geology 2:71–74

Colman SM, Baucom PC, Bratton JF et al (2002) Radiocarbon dating, chronologic framework, and changes in accumulation rates of Holocene estuarine sediments from Chesapeake Bay. Quat Res 57:58–70. https://doi.org/10.1016/j.yqres.2003.11.004

Conley DJ (1997) Riverine contribution of biogenic silica to the oceanic silica budget. Limnol. Oceanogr 42:774–777

Conley DJ (1998) An interlaboratory comparison for the measurement of biogenic silica in sediments. Mar Chem 63:39–48. https://doi.org/10.1016/S0304-4203(98)00049-8

Conley DJ (2002) Terrestrial ecosystems and the global biogeochemical silica cycle. Global Biogeochem Cycles 16:68. https://doi.org/10.1029/2002GB001894

Conley DJ, Malone TC (1992) Annual cycle of dissolved silicate in Chesapeake Bay : implications for the production and fate of phytoplankton biomass. Mar Ecol Prog Ser 81:121–128

Conley DJ, Schelske CL (2001) Biogenic silica. In: Smol JP, Birks HJB, Last WM (eds) Tracking environmental change using lake sediments. Terrestrial, algal, and siliceous indicators, vol 3, 3rd edn. Kluwer, Dordrecht, pp 281–293

Conley DJ, Schelske CL, Stoermer EF (1993) Modification of the biogeochemical cycle of silica with eutrophication. Mar Ecol Prog Ser 101:179–192. https://doi.org/10.3354/meps101179

Conley DJ, Kaas H, Møhlenberg F et al (2000) Characteristics of Danish Estuaries. Estuaries 23:820. https://doi.org/10.2307/1353000

Conley DJ, Likens GE, Buso DC et al (2008) Deforestation causes increased dissolved silicate losses in the Hubbard Brook Experimental Forest. Glob Chang Biol 14:2548–2554. https://doi.org/10.1111/j.1365-2486.2008.01667.x

Cooper SR (1995) Chesapeake Bay watershed historical land use: impact on water quality and diatom communities. Ecol Appl 5:703–723

Cooper SR, Brush GS (1993) A 2500-year history of anoxia and eutrophication in Chesapeake Bay. Estuaries 16:617–626

Cornelis JT, Delvaux B, Cardinal D et al (2010) Tracing mechanisms controlling the release of dissolved silicon in forest soil solutions using Si isotopes and Ge/Si ratios. Geochim Cosmochim Acta 74:3913–3924. https://doi.org/10.1016/j.gca.2010.04.056

Cornwell JC, Conley DJ, Owens M, Stevenson JC (1996) A Sediment Chronology of the Eutrophication of Chesapeake Bay. Estuaries 19:488–499. https://doi.org/10.2307/1352465

Correll DL, Jordan TE, Weller DE (2000) Dissolved silicate dynamics of the Rhode River watershed and estuary. Esturies 23:188–198

Cronin TM, Vann CD (2003) The sedimentary record of climatic and anthropogenic influence on the Patuxent estuary and Chesapeake Bay ecosystems. Estuaries 26:196–209. https://doi.org/10.1007/BF02695962

Cronin TM, Willard D, Karlsen A et al (2000) Climatic variability in the eastern United States over the past millenium from Chesapeake Bay sediments. Geology 28:3–6. https://doi.org/10.1130/0091-7613(2000)28%3c3

Cronin TM, Dwyer GS, Kamiya T et al (2003) Medieval warm period, little ice age and 20th century temperature variability from Chesapeake Bay. Glob Planet Change 36:17–29. https://doi.org/10.1016/S0921-8181(02)00161-3

Cronin TM, Thunell R, Dwyer GS et al (2005) Multiproxy evidence of Holocene climate variability from estuarine sediments, eastern North America. Paleoceanography. https://doi.org/10.1029/2005PA001145

Cronin TM, Vogt PR, Willard DA et al (2007) Rapid sea level rise and ice sheet response to 8200-year climate event. Geophys Res Lett 34:L20603. https://doi.org/10.1029/2007GL031318

D'Elia CF, Nelson DM, Boynton WR (1983) Chesapeake Bay nutrient and plankton dynamics: III. The annual cycle of

dissolved silicon. Geochemica Cosmochim Acta 47:1945–1955

De la Rocha CL, Brzezinski MA, DeNiro MJ (1997) Fractionation of silicon isotopes by marine diatoms during biogenic silica formation. Geochim Cosmochim Acta 61:5051–5056. https://doi.org/10.1016/S0016-7037(97)00300-1

De La Rocha CL, Brzezinski MA, DeNiro MJ (2000) A first look at the distribution of the stable isotopes of silicon in natural waters. Geochim Cosmochim Acta 64:2467–2477. https://doi.org/10.1016/S0016-7037(00)00373-2

Delvaux C, Cardinal D, Carbonnel V et al (2013) Controls on riverine d30Si signatures in a temperate watershed under high anthropogenic pressure (Scheldt—Belgium). J Mar Syst 128:40–51. https://doi.org/10.1016/j.jmarsys.2013.01.004

DeMaster DJ (1981) The supply and accumulation of silican in the marine environment. Geochemica Cosmochim 45:1715–1732

DeMaster DJ (2002) The accumulation and cycling of biogenic silica in the Southern Ocean: revisiting the marine silica budget. Deep Res II 49:3155–3167. https://doi.org/10.1016/S0967-0645(02)00076-0

Dettmann EH (2001) Effect of water residence time on annual export and denitrification of nitrogen in estuaries: a model analysis. Estuaries 24:481–490. https://doi.org/10.2307/1353250

Ding T, Wan D, Wang C, Zhang F (2004) Silicon isotope compositions of dissolved silicon and suspended matter in the Yangtze River, China. Geochim Cosmochim Acta 68:205–216. https://doi.org/10.1016/S0016-7037(03)00264-3

Du J, Shen J (2016) Water residence time in Chesapeake Bay for 1980–2012. J Mar Syst 164:101–111

Dürr HH, Meybeck M, Hartmann J et al (2011) Global spatial distribution of natural riverine silica inputs to the coastal zone. Biogeosciences 8:597–620. https://doi.org/10.5194/bg-8-597-2011

Eggimann DW, Manheim FT, Betzer PR (1980) Dissolution and analysis of amorphous silica in marine sediments. J Sediment Petrol 50:215–225. https://doi.org/10.1306/212F79AF-2B24-11D7-8648000102C1865D

Fisher TR, Gustafson AB, Sellner K et al (1999) Spatial and temporal variation of resource limitation in Chesapeake Bay. Mar Biol 133:763–778. https://doi.org/10.1007/s002270050518

Frings PJ, Clymans W, Jeppesen E et al (2014a) Lack of steady-state in the global biogeochemical Si cycle: emerging evidence from lake Si sequestration. Biogeochemistry 117:255–277. https://doi.org/10.1007/s10533-013-9944-z

Frings PJ, De La Rocha CL, Struyf E et al (2014b) Tracing silicon cycling in the Okavango Delta, a sub-tropical flood-pulse wetland using silicon isotopes. Geochim Cosmochim Acta 142:132–148. https://doi.org/10.1016/j.gca.2014.07.007

Frings PJ, Clymans W, Fontorbe G et al (2016) The continental Si cycle and its impact on the ocean Si isotope budget. Chem Geol 425:12–36. https://doi.org/10.1016/j.chemgeo.2016.01.020

Georg RB, Reynolds BC, Frank M, Halliday AN (2006) New sample preparation techniques for the determination of Si isotopic compositions using MC-ICPMS. Chem Geol 235:95–104. https://doi.org/10.1016/j.chemgeo.2006.06.006

Georg RB, West AJ, Basu AR, Halliday AN (2009) Silicon fluxes and isotope composition of direct groundwater discharge into the Bay of Bengal and the effect on the global ocean silicon isotope budget. Earth Planet Sci Lett 283:67–74. https://doi.org/10.1016/j.epsl.2009.03.041

Hagy JD, Bounton WR, Keefe CW, Wood KV (2004) Hypoxia in Chesapeake Bay, 1950–2001: long-term change in relation to nutrient loading and river flow. Estuaries 27:634–658

Hagy JD, Boynton WR, Jasinski DA (2005) Modelling phytoplankton deposition to Chesapeake Bay sediments during winter-spring: interannual variability in relation to river flow. Estuar Coast Shelf Sci 62:25–40. https://doi.org/10.1016/j.ecss.2004.08.004

Honjo S, Manganini SJ, Krishfield RA, Francois R (2008) Particulate organic carbon fluxes to the ocean interior and factors controlling the biological pump: a synthesis of global sediment trap programs since 1983. Prog Oceanogr 76:217–285. https://doi.org/10.1016/j.pocean.2007.11.003

Hughes HJ, Bouillon S, André L, Cardinal D (2012) The effects of weathering variability and anthropogenic pressures upon silicon cycling in an intertropical watershed (Tana River, Kenya). Chem Geol 308–309:18–25. https://doi.org/10.1016/j.chemgeo.2012.03.016

Hurrell JW (1995) Decadal trends in the North Atlantic Oscillation: regional temperatures and precipitation. Science 80(269):676–679. https://doi.org/10.1126/science.269.5224.676

Jickells TD (1998) Nutrient biogeochemistry of the coastal zone. Science 80(281):217–222. https://doi.org/10.1126/science.281.5374.217

Kaushal S, Binford MW (1999) Relationship between C: N ratios of lake sediments, organic matter sources, and historical deforestation in Lake Pleasant, Massachusetts, USA. J Paleolimnol 22:439–442. https://doi.org/10.1023/A:1008027028029

Kemp WM, Boynton WR, Adolf JE et al (2005) Eutrophication of Chesapeake Bay: historical trends and ecological interactions. Mar Ecol Prog Ser 303:1–29. https://doi.org/10.3354/meps303001

Krause JW, Darrow ES, Pickering RA et al (2017) Reactive silica fractions in coastal lagoon sediments from the northern Gulf of Mexico. Cont Shelf Res 151:8–14. https://doi.org/10.1016/j.csr.2017.09.014

Laruelle GG, Roubeix V, Sferratore A et al (2009) Anthropogenic perturbations of the silicon cycle at the global scale: key role of the land-ocean transition. Global Biogeochem Cycles 23:1–17. https://doi.org/10.1029/2008GB003267

Leng MJ, Swann GEA, Hodson MJ et al (2009) The potential use of silicon isotope composition of biogenic silica as a proxy for environmental change. Silicon 1:65–77. https://doi.org/10.1007/s12633-009-9014-2

Luu TNM, Garnier J, Billen G et al (2012) N, P, Si budgets for the Red River Delta (northern Vietnam): how the delta affects river nutrient delivery to the sea. Biogeochemistry 107:241–259. https://doi.org/10.1007/s10533-010-9549-8

Mackey EA, Christopher SJ, Lindstrom RM et al (2010) Certification of Three NIST Renewal Soil Standard Reference Materials for Element Content : SRM 2709a San Joaquin Soil, SRM 2710a Montana Soil I, and SRM 2711a Montana Soil II. Natl Inst Stand Technol Spec Publ 260:1–39

Maher K, Chamberlain CP (2014) Hydrologic regulation of chemical. Science 80(343):1502–1504. https://doi.org/10.1126/science.1250770

Malone TC, Conley DJ, Fisher TR et al (1996) Scales of nutrient-limited phytoplankton productivity in Chesapeake Bay. Estuaries 19:371. https://doi.org/10.2307/1352457

Mangalaa KR, Cardinal D, Brajard J et al (2017) Silicon cycle in Indian estuaries and its control by biogeochemical and anthropogenic processes. Cont Shelf Res 148:64–88. https://doi.org/10.1016/j.csr.2017.08.011

Marshall HG, Lacouture RV, Buchanan C, Johnson JM (2006) Phytoplankton assemblages associated with water quality and salinity regions in Chesapeake Bay, USA. Estuar Coast Shelf Sci 69:10–18. https://doi.org/10.1016/j.ecss.2006.03.019

Meybeck M, Vörösmarty C (2005) Fluvial filtering of land-to-ocean fluxes: from natural Holocene variations to Anthropocene. Compt Rend Geosci 337:107–123. https://doi.org/10.1016/j.crte.2004.09.016

Meyers PA, Lallier-Verges E (1999) Lacustrine sedimentary organic matter records of Late Quaternary paleoclimates. J Paleolimnol 21:345–372. https://doi.org/10.15530/urtec-2016-2461914

Morley DW, Leng MJ, Mackay AW et al (2004) Cleaning of lake sediment samples for diatom oxygen isotope analysis. J Paleolimnol 31:391–401

Niencheski LFH, Windom HL, Moore WS, Jahnke RA (2007) Submarine groundwater discharge of nutrients to the ocean along a coastal lagoon barrier, Southern Brazil. Mar Chem 106:546–561. https://doi.org/10.1016/j.marchem.2007.06.004

Oelze M, Schuessler JA, Von Blanckenburg F (2016) Mass bias stabilization by Mg doping for Si stable isotope analysis by MC-ICP-MS. J Anal At Spectrom 31:2094–2100. https://doi.org/10.1039/C6JA00218H

Opfergelt S, Georg RB, Delvaux B et al (2012) Silicon isotopes and the tracing of desilication in volcanic soil weathering sequences, Guadeloupe. Chem Geol 326–327:113–122. https://doi.org/10.1016/j.chemgeo.2012.07.032

Pasternack GB, Brush GS, Hilgartner WB (2001) Impact of historic land-use change on sediment delivery to a Chesapeake Bay subestuarine delta. Earth Surf Process Landforms 26:409–427

Ragueneau O, Gallinari M, Corrin L et al (2001) The benthic silica cycle in the Northeast Atlantic: annual mass balance, seasonality, and importance of non-steady-state processes for the early diagenesis of biogenic opal in deep-sea sediments. Prog Oceanogr 50:171–200. https://doi.org/10.1016/S0079-6611(01)00053-2

Rahman S, Aller RC, Cochran JK (2017) The missing silica sink: revisiting the marine sedimentary Si cycle using cosmogenic 32Si. Global Biogeochem Cycles 31:1559–1578. https://doi.org/10.1002/2017GB005746

Rahman S, Tamborski JJ, Charette MA, Cochran JK (2019) Dissolved silica in the subterranean estuary and the impact of submarine groundwater discharge on the global marine silica budget. Mar Chem 208:29–42

Reynolds BC, Aggarwal J, André L et al (2007) An inter-laboratory comparison of Si isotope reference materials. J Anal At Spectrom 22:561–568. https://doi.org/10.1039/B616755A

Saenger C, Cronin T, Thunell R, Vann C (2006) Modelling river discharge and precipitation from estuarine salinity in the northern Chesapeake Bay: application to Holocene palaeoclimate. The Holocene 16:467–477

Sauer D, Saccone L, Conley DJ et al (2006) Review of methodologies for extracting plant-available and amorphous Si from soils and aquatic sediments. Biogeochemistry 80:89–108. https://doi.org/10.1007/s10533-005-5879-3

Savage PS, Armytage RMG, Georg RB, Halliday AN (2014) High temperature silicon isotope geochemistry. Lithos 190–191:500–519. https://doi.org/10.1016/j.lithos.2014.01.003

Siipola V, Lehtimäki M, Tallberg P (2016) The effects of anoxia on Si dynamics in sediments. J Soils Sediment 16:266–279. https://doi.org/10.1007/s11368-015-1220-5

Struyf E, Conley DJ (2012) Emerging understanding of the ecosystem silica filter. Biogeochemistry 107:9–18. https://doi.org/10.1007/s10533-011-9590-2

Struyf E, Smis A, Van Damme S et al (2009) The global biogeochemical silicon cycle. Silicon 1:207–213. https://doi.org/10.1007/s12633-010-9035-x

Struyf E, Smis A, Van Damme S et al (2010) Historical land use change has lowered terrestrial silica mobilization. Nat Commun 129:1–7. https://doi.org/10.1038/ncomms1128

Sun X, Andersson P, Humborg C et al (2011) Climate dependent diatom production is preserved in biogenic Si isotope signatures. Biogeosciences 8:3491–3499. https://doi.org/10.5194/bg-8-3491-2011

Sun X, Olofsson M, Andersson PS et al (2014) Effects of growth and dissolution on the fractionation of silicon isotopes by estuarine diatoms. Geochim Cosmochim Acta 130:156–166. https://doi.org/10.1016/j.gca.2014.01.024

Sutton JN, Varela DE, Brzezinski MA, Beucher CP (2013) Species-dependent silicon isotope fractionation by marine diatoms. Geochim Cosmochim Acta 104:300–309. https://doi.org/10.1016/j.gca.2012.10.057

Tréguer PJ, De La Rocha CL (2013) The world ocean silica cycle. Ann Rev Mar Sci 5:477–501. https://doi.org/10.1146/annurev-marine-121211-172346

Van Dam H, Mertens A, Sinkeldam J (1994) A coded checklist and ecological indicator values of freshwater diatoms from The Netherlands. Netherlands J Aquat Ecol 28:117–133. https://doi.org/10.1007/BF02334251

Vandevenne FI, Delvaux C, Hughes HJ et al (2015) Landscape cultivation alters δ^{30}Si signature in terrestrial ecosystems. Sci Rep. https://doi.org/10.1038/srep07732

Varela DE, Pride CJ, Brzezinski MA (2004) Biological fractionation of silicon isotopes in Southern Ocean surface waters. Global Biogeochem Cycles 18:1–8. https://doi.org/10.1029/2003GB002140

Vega AJ, Rohli RV, Sui CH (1999) Climatic relationships to Chesapeake Bay salinity during southern oscillation extremes. Phys Geogr 20:468–490

Villnäs A, Norkko J, Lukkari K et al (2012) Consequences of increasing hypoxic disturbance on benthic communities and ecosystem functioning. PLoS ONE. https://doi.org/10.1371/journal.pone.0044920

Walker JCG, Hays PB, Kasting JF (1981) A negative feedback mechanism for the long-term stabilization of earth's surface temperature. J Geophys Res 86:9776–9782

Willard DA, Cronin TM, Verardo S (2003) Late-Holocene climate and ecosystem history from Chesapeake Bay sediment cores, USA. The Holocene 2:201–214

Willard DA, Bernhardt CE, Korejwo DA, Meyers SR (2005) Impact of millennial-scale Holocene climate variability on eastern North American terrestrial ecosystems: pollen-based climatic reconstruction. Glob Planet Change 47:17–35. https://doi.org/10.1016/j.gloplacha.2004.11.017

Willard DA, Bernhardt CE, Hupp CR, Newell WN (2015) Coastal and wetland ecosystems of the Chesapeake Bay watershed: applying palynology to understand impacts of changing climate, sea level, and land use. Am F Guid 40:281–308. https://doi.org/10.1130/2015.0040

Zhang J, Liu SM, Ren JL et al (2007) Nutrient gradients from the eutrophic Changjiang (Yangtze River) Estuary to the oligotrophic Kuroshio waters and re-evaluation of budgets for the East China Sea Shelf. Prog Oceanogr 74:449–478. https://doi.org/10.1016/j.pocean.2007.04.019